Used Fuel Integrity Program: Summary Report

NWMO TR-2011-04 **February 2011**

Jose Freire-Canosa

Nuclear Waste Management Organization

nwmo

NUCLEAR WASTE MANAGEMENT ORGANIZATION
SOCIÉTÉ DE GESTION DES DÉCHETS NUCLÉAIRES

Nuclear Waste Management Organization
22 St. Clair Avenue East, 6th Floor
Toronto, Ontario
M4T 2S3
Canada

Tel: 416-934-9814
Web: www.nwmo.ca

Used Fuel Integrity Program: Summary Report

NWMO TR-2011-04

February 2011

Jose Freire-Canosa
Nuclear Waste Management Organization

ABSTRACT

Title: **Used Fuel Integrity Program: Summary Report**
Report No.: **NWMO TR-2011-04**
Author(s): Jose Freire-Canosa
Company: Nuclear Waste Management Organization
Date: February 2011

Abstract
When CANDU fuel bundles are removed from a nuclear reactor, they are stored on an interim basis in wet storage bays for a period of about seven to ten years and then transferred to licensed dry storage facilities at the reactor site while awaiting the development of a deep geological repository for long-term management. The majority of used fuel in dry storage in Canada is in the Dry Storage Containers (DSCs) developed by Ontario Power Generation.

During the period of dry storage, several mechanisms such as creep rupture, stress corrosion cracking and delayed hydride cracking could potentially affect the integrity of the CANDU fuel bundles. The Used Fuel Integrity Program was established in 2004 to improve our understanding of processes that could affect fuel bundle integrity and to assess whether those processes pose a risk of mechanical failure of the fuel bundles in dry storage. The most important threat to CANDU fuel bundle integrity was found to be Delayed Hydride Cracking (DHC) of the endplate / endcap welds which could lead to mechanical failure of the bundle welds.

This report provides a summary of the Used Fuel Integrity Program and the key findings of the work. A Finite Element Model (FEM) of the CANDU fuel bundle was developed and tested to predict fuel bundle stress fields following its post-in-reactor life. The "Bundle Stress Model" was created with the ANSYS code as a parametric model which allows for ease of simulating various fuel bundle load conditions and bundle deformations. Solutions obtained with the model were verified against test measurements of the deformations experienced by unirradiated commercial bundles subjected to various load conditions. Loads applied to the fuel bundles tested covered both linear elastic and plastic stress regimes. The Bundle Stress Model provided excellent trending of the data and good reproducibility of the test data.

Concurrent with the development of the Bundle Stress Model, laboratory experiments were done with unirradiated endplate/endcap welds from artificially hydrided CANDU fuel bundles to hydrogen levels of 40-60 ppm. The intent was to obtain a database of threshold stress intensity factors (K_{IH}) which would lead to DHC failure of the welds. The values of this database were then used to compare against the stress intensity factors expected to be operative at the welds as estimated from the field stresses calculated with the "Bundle Stress Model".

The results of this evaluation indicate that maximum stress intensity factors of the order of 3 MPa $m^{1/2}$ are expected for 28-element Pickering type CANDU fuel bundles when radiation effects are factored in. The database from the experimental program indicates that the threshold stress intensity factor for DHC crack initiation is in the range 7.6 to 13.6 MPa $m^{1/2}$. Therefore, DHC is not projected to occur and the bundles are expected to retain their integrity during dry storage. Similar results are expected for the 37-element Bruce type CANDU fuel bundles.

TABLE OF CONTENTS

LIST OF TABLES

Page

LIST OF FIGURES

Page

1. INTRODUCTION

Since the introduction of commercial nuclear power in Canada, used CANDU nuclear fuel have been steadily accumulating at the various reactor sites. As of June 30, 2010, about 2.2 million spent fuel bundles are in storage at both waterpools and dry storage facilities. The number of fuel bundles in waterpools is about 1.5 million and in dry storage about 0.6 million bundles.

Used CANDU fuel could be in interim dry storage facilities for a period of up to 100 years before being placed in a deep geological repository (DGR) for long-term management. Before transfer to the deep repository, the condition of the fuel should remain intact or suffer little, if any, degradation during its interim storage phase. Of particular importance, is the mechanical integrity of the fuel bundle assembly and the condition of the fuel elements cladding.

The fuel cladding offers containment of the fission products produced during irradiation and acts as a barrier to radionuclide release. Fuel cladding integrity is important since a breached fuel cladding would potentially lead to contamination during handling and fuel transportation. Used fuel bundle arrays that contain endplate / endcap welds that are broken would have loose fuel pencils or elements which if located in the outer ring of the fuel bundle array may lead to inefficient handling of the fuel bundles during fuel bundle transfer operations.

During the used fuel bundle storage phase, a number of mechanisms that could lead to the deterioration of the bundles by breaching their fuel elements cladding and/or failure of the endplate/endcap welds have been identified. Among these, fracture of the cladding by Stress Corrosion Cracking (SCC) by iodine or liquid metal embrittlement by cesium and/or cadmium have been postulated and studied. Delayed Hydride Cracking (DHC) of the endplate/endcap welds leading to fracture was identified as being of particular concern to CANDU fuel stored in dry storage on a horizontal (or laying on its side orientation) as with fuel stored in modules in the Ontario Power Generation Dry Storage Containers or DSCs. Additionally, the release of gaseous and volatile fission products during the fuel in-reactor life leads to the internal pressurization of the fuel elements. This increase in the internal pressure of the fuel elements could conceivably lead to creep rupture of the fuel cladding. Fast fracture of the clad might also be a consideration.

The Nuclear Waste Management Organization (NWMO) and its member organizations assessed these postulated used fuel degradation mechanisms and established the Used Fuel Integrity (UFI) Program in 2004 to address these concerns. The UFI Program built on Atomic Energy of Canada Limited's (AECL's) previous research work on the behaviour of used CANDU fuel in wet and dry storage dating back to 1979.

Work undertaken in the UFI Program established that DHC of the endplate/endcap welds of CANDU fuel bundles is potentially the most likely operative mechanism to affect bundles integrity during dry storage. This report summarizes the work and the findings of the study.

2. USED FUEL STORAGE: CURRENT STATUS

2.1 WET STORAGE

Used CANDU fuel is stored under water in waterpools following discharge from the reactor. After seven to ten years of storage at the waterpool, the used fuel may be transferred to dry storage depending on the fuel management operations at the station site. The integrity of the fuel cladding during waterpool storage is of primary importance to ensure that the fuel cladding is not breached leading to the release of radionuclides contained in the fuel. The corrosion performance of the fuel is monitored and the chemistry of the pool water is controlled within established specifications to ensure the longevity of the fuel cladding, and, to ensure the safe operation of the waterpools.

Table 1: Summary of Nuclear Fuel Waste in Canada as of June 30, 2010

Location	Waste Owner	Wet Storage (# bundles)	Dry Storage (# bundles)	TOTAL (# bundles)
Bruce A	OPG	364,381	46,464	410,845
Bruce B	OPG	375,566	145,912	521,478
Darlington	OPG	329,198	48,363	377,561
Douglas Point	AECL	0	22,256	22,256
Gentilly 1	AECL	0	3,213	3,213
Gentilly 2	HQ	29,833	86,340	116,173
Pickering A	OPG	401,737	214,436	616,173
Pickering B	OPG			
Point Lepreau	NBPN	40,758	81,000	121,758
AECL Whiteshell	AECL	0	2,268	2,268
AECL Chalk River	AECL	0	4,886	4,886
	TOTAL	**1,541,473**	**655,138**	**2,196,611**

Notes: 1) AECL = Atomic Energy of Canada Limited;
HQ = Hydro-Québec;
NBPN = New Brunswick Power Nuclear;
OPG = Ontario Power Generation Inc.

2) 360 bundles of Whiteshell fuel are standard CANDU bundles. The remaining bundles are various research, prototype and test fuel bundles, similar in size and shape to standard CANDU bundles.

Currently, used fuel from Canadian reactors stored in the waterpools amount to about 2.2 million bundles. Dry storage of the fuel has become the preferred mode of storage, following a period of seven to ten years of storage at the waterpool. Table 1 provides a breakdown of fuel being stored at the various sites in Canada in both wet and dry storage facilities as of June 30, 2010 (Garamszeghy, 2010). These numbers exclude the fuel resident in the reactors as of June 30, 2010 and also small quantities of non-standard experimental fuels currently in storage at AECL's Chalk River Laboratories.

Jointly, AECL and Ontario Hydro (which became Ontario Power Generation) undertook a research program in 1979 to monitor typical used fuel including commercial CANDU fuel stored under water for over twenty years to detect any degradation mechanisms which could impact the integrity of the fuel over long term storage in the waterpool. Periodically, fuel was examined and designated fuel elements investigated though destructive testing to determine if any significant deterioration was occurring. After twenty seven years in storage, the conclusion of this monitoring was that the fuel had not experienced any significant deterioration and fuel would be expected to last without significant degradation beyond a fifty year storage period in the waterpools (Wasywich and Frost, 1991; Hunt et al, 1982). Additionally, AECL also tested irradiated fuel cladding from commercial fuel for susceptibility to Stress Corrosion Cracking (SCC) by iodine and liquid metal embrittlement by Cesium and Cadmium. The overall conclusion was that these particular mechanisms of fuel clad degradation will not lead to fuel cladding failure of commercial CANDU fuel (Hunt et al, 1982).

2.2 DRY STORAGE

Since the early 1990's, a trend to store commercial used fuel dry became established. In Canada, several concepts were developed and are in current use. The CANSTOR system developed by AECL is primarily a modular reinforced concrete vault where the used fuel is first encapsulated in a cylindrical C-steel container and the containers stacked in cylindrical C-steel tubes inside the vault. The concrete vault provides shielding from the used fuel radiation. The concrete vault also allows for passive dissipation of the heat from the stored used fuel through convection. The used fuel storage temperature is about 60°C. Since the vault is designed modularly, expansion of the CANSTOR system storage capacity is achieved by adding additional vault modules. This system of storage is well established and is the system of choice at Hydro-Québec at their Gentilly site in Trois-Rivières.

Earlier in the mid-1970's, AECL also developed reinforced concrete canisters for the storage of the used fuel being used in the Whiteshell Research Establishment at Pinawa, Manitoba. The concrete canisters are concrete reinforced monoliths built on reinforced concrete pads. The concrete canisters are provided with an inner C-steel tube which serves both as a concrete form during pouring of the concrete during the canister manufacturing process and, later, as the enclosure for storing the used fuel. As in the case of the CANSTOR system, fuel is first transferred from the waterpool into stainless steel baskets in a dry mode. The metallic baskets are then seal welded and transferred to the concrete canister for storage. A reinforced concrete plug is used to cap the concrete canister and secure in place usually by welding it to the concrete canister. The concrete canister provides both containment and radiation shielding for the stored fuel. This mode of storage is in use at the AECL facilities (Whiteshell and Chalk River Laboratories) and commercially at the New Brunswick's Point Lepreau site.

In the 1990's, Ontario Hydro (now Ontario Power Generation Inc. (OPG) developed a steel and reinforced concrete container known as the Dry Storage Container or DSC which is licensed for both used fuel storage and transportation. The DSC has an inner and outer C-steel liner entirely enclosing the reinforced concrete structure. A lid in the form of a reinforced concrete structure encased in a C-steel liner is also provided. The outer shape of the DSC is cylindrical but its inner cavity is rectangular to match the shape and size of the OPG waterpool storage modules. The storage modules are optimized storage baskets for the used fuel designed to hold 96 CANDU fuel bundles and maximize the storage capacity of OPG waterpools. One DSC holds four storage modules or 384 used fuel bundles. Once loaded with fuel, the lid is hermetically attached to the base of the DSC by multiple pass weldments. In the OPG DSCs, the void space inside the DSC is filled with helium and the fuel temperatures are at about 150^{o}C or lower.

Table 1 details the breakdown of fuel accumulations in dry storage at the various sites. The total amount of fuel in dry storage is about 655,000 bundles or 13,000 Mg of uranium dioxide. The most fuel is stored in DSCs, followed by the CANSTOR system in an approximate ratio of 6 to 1. Since the mid-nineties, increased used fuel storage capacity needs world-wide are being met with dry storage.

3. USED CANDU FUEL INTEGRITY PROGRAM: SCOPE

3.1 LONG-TERM MANAGEMENT OF THE USED FUEL DATABASE

Currently, all information related to the used fuel bundles including manufacturing and irradiation history information resides with the commercial nuclear stations at the various sites. Fuel data for early reactors and prototypes resides with AECL. In Canada, two prototypes for commercial production of electrical power were developed and operated: The Nuclear Power Development (NPD) reactor and the Douglas Point reactor. Both are currently decommissioned and all their fuel dry stored on-site in AECL concrete canisters.

The NPD reactor was tested and operated at Rolphton (Ont.) from 1962-1987 as the first prototype of the heavy water CANDU reactor. It produced 22 MW of electrical power and was mainly dedicated for proving the feasibility of producing competitive priced power from the nuclear fission of uranium-235. In this way, a new reactor using pressure tubes rather than a pressure vessel with on-line refuelling of the fuel in the pressure tubes was developed as a distinctively new Canadian technological achievement. The Douglas Point reactor located at the Bruce site and producing 200 MW of electrical power was a scale-up version of the NPD reactor that established the CANDU reactor as a commercially viable nuclear power system. Both reactors were operated for several decades and decommissioned in the mid-1980's after serving for research, data collection and the training of operators for the current fleet of CANDU reactors.

As both the amount of fuel in storage continues to increase and the storage times get extended into the future, means for securing the information about the fuel for the long term becomes more important. As part of the UFI Program, the type of data that should be preserved and the means for preserving have been assessed. There is also a growing international effort to assess this issue, and the International Atomic Energy Agency (IAEA) has taken a specific interest in it. To address these concerns, the NWMO has proceeded to identify the minimum

data requirements that would need to be kept for future generations. It has also identified electronic storage and paper as the best media to preserve the current available data. Additionally, a recommendation was proposed to conduct a trial run at a designated nuclear station for the purpose of assessing the ease of data availability on stored fuel at the station to confirm the condition of the data and its transfer requirements to centralize it at a future date.

3.2 USED FUEL INTEGRITY POSTULATED DEGRADATION PROCESSES

After the fuel has been irradiated in a reactor, the material components of the fuel have been affected by irradiation. The fission processes result in the formation of radionuclides or fission products in the form of gases, volatiles and solid phase particles that remain contained in the fuel pellets and the fuel elements. Additionally, the high temperatures experienced by the fuel during radiation contribute to thermo-mechanical stresses that may lead to mechanical deformations – albeit nearly imperceptible - of the elements and the fuel assembly.

Since the bundle remains a dynamic entity due to the steady decay of the radionuclides and the heat power of decay, a number of processes have been speculated as to whether they could have an impact on the long-term behaviour of the fuel as follows:

a. Fuel cladding oxidation

b. Fast fracture

c. Creep

d. Stress Corrosion Cracking (SCC)

e. Liquid Metal Embrittlement by Cs and Cd

f. Delayed Hydride Cracking (DHC)

The possibility that any of these processes might contribute to the degradation of the fuel has been studied for CANDU fuel since the early 1980's. Results from these studies indicate that for the conditions of storage, these processes are not expected to have an impact on the long-term condition of the fuel.

Early studies by Byrne and Freire-Canosa (1984) and Hunt et al. (1981) addressed the potential impact of these postulated mechanisms on the long-term integrity of the fuel. The Byrne and Freire-Canosa analysis concluded that for fuel dry stored at temperatures below 200^{o}C:

1. Oxidation of the cladding when the fuel is exposed to air was found to be negligible. A 0.04% thickness loss of the cladding thickness was predicted for the first 100 years of storage and 0.4% in 1000 years.

2. Failure of cladding due to fast fracture by plastic collapse will be insignificant. Typical bundles representative of the CANDU fuel population will only fail if cracks with a depth of 92 per cent of the cladding thickness are present.

3. Failure by fast fracture occurs preferentially by plastic collapse rather than brittle fracture.

4. Typical CANDU fuel will be unaffected by stress rupture for at least 10^6 years.

5. Migration of hydrogen to the endplate/endcap welds is negligible and will not contribute significantly to a decrease in its mechanical strength.

Hunt et al. (1981) developed a database for both SSC by iodine and Liquid Metal Embrittlement by Cs and Cd of the Zircaloy cladding by stressing irradiated fuel cladding rings. The results of those tests indicated that unless a 95% through the wall crack is already present in the cladding, an unlikely event, both SCC and Liquid Metal Embrittlement will not be operative at the higher temperatures of storage relevant to dry storage of CANDU fuel.

Uniform corrosion of the cladding was also assessed by Ikeda (2002). The results of this assessment indicated that the cladding can be expected to remain intact for at least 300 years. Further, Ikeda also concluded that localized corrosion by mechanisms such as crevice corrosion and Stress Corrosion Cracking were not a concern. Cann and Tait (2002) also studied the impact of creep on fuel in dry storage and concluded that for at least 300 years, creep will not be operative.

The potential for Delayed Hydride Cracking (DHC) of the cladding was also assessed. While the migration of hydrogen/deuterium to the endplate/endcap weldments was found to be negligible by Byrne and Freire-Canosa, it was considered that the potential existed for DHC to be operative at the endplate/endcap weldments on the CANDU fuel bundle due to mechanical loading during the fuel dry storage phase. As a result of this conclusion, a program was launched to assess this possibility. The results of this study are summarized in this report.

3.2.1 Bundle Stress Model

The activation of Delayed Hydride Cracking is sensitive to stresses. Hydrogen migrates to areas of high stress where it can precipitate in the form of metallic hydrides depending on the solubility curve for hydride formation. During storage in a DSC, the fuel temperature is raised to about 150°C from the 20-30°C temperature of wet storage at the waterpools. The higher temperature re-dissolves the hydrides present in the cladding during wet storage and the hydrogen is free to migrate to areas of high stresses where it can re-precipitate as hydrides when the fuel subsequently cools down during dry storage.

For Delayed Hydride Cracking to occur at the endplate / endcap welds, the stress intensity factors at the welds will have to be above the threshold stress intensity factor (K_{IH}) for DHC to proceed. The CANDU fuel bundle endplate/endcap welds are characterized by the presence of a notch of about 10μm radius that acts as a stress raiser. As a result, being able to determine the stress fields in a bundle after its post-reactor life is important in assessing whether DHC might be an operative mechanism. In particular, the operating stresses at the endplate/endcap welds are of particular importance.

In order to obtain a description of the stress fields that might be present in a bundle post-reactor, a finite element model (FEM) of the whole bundle assembly was developed using the software platform ANSYS. The FEM model known as the Bundle Stress Model is capable of predicting the stresses in the bundle when subjected to various deformations. The deformations

can be made to replicate those commonly observed through PIE examinations of bundles after post-reactor discharge. In this way, stresses in the endplate/endcap region of the welds can be estimated. These values are then used to derive stress intensity factors at the endplate/endcap welds. The calculated values can then be compared with experimentally found threshold stress intensity factors or K_{IH} that are observed for delayed hydride cracking. The comparison provides information to assess whether DHC is likely to occur for the CANDU fuel bundles in dry storage.

3.2.2 Delayed Hydride Cracking of Endplate/Endcap Welds

In the reactor, the Zircaloy components of the CANDU fuel bundle such as the cladding, endplates, endcaps and bearing pads, pick-up hydrogen mainly through corrosion of the Zircaloy. The hydrogen precipitates as hydrides within the metallic matrix. The fuel bundle operates at a much higher temperature in the reactor corresponding to a much higher solubility of the hydrides. On discharge to the waterpool, the soluble hydrogen precipitates at the much lower temperature.

While Delayed Hydride Cracking has not been observed at the operating temperature of the waterpools, on re-storing the fuel in a Dry Storage Container, the temperature of the bundle is increased from that at the waterpool to about 150^{o}C in the dry storage system. The result is that hydrides that precipitated on cooling at the waterpool temperature re-dissolve and are available for mobility within the metallic matrix. Movement can be realized both down temperature and stress gradients. In storage systems where the CANDU fuel bundle is stored in a vertical position, i.e., sitting on one of the endplates, migration of the hydrides to the endplate/endcap welds is not viewed as occurring since the stresses remain compressive at the endcap/endplate welds and fracture propagation would not be expected. However, storage of the CANDU fuel in a horizontal position as is the case in the Dry Storage Containers, the weight of the bundle rests on two or four endplate/endcap welds on a tensional field that can lead to stress gradients that can preferentially attract the migration of the hydrides to this preferred location, and, consequently lead to Delayed Hydride Cracking at the notch present at the weld. Hence, determination of the threshold stress intensity factors at the endplate/endcap welds experimentally at the temperature of storage is important to elucidate whether DHC is operative in CANDU fuel bundles. In order to study this phenomenon for CANDU fuel, an appropriate experimental set-up had to be developed and tested to ensure its workability. Test results will be discussed below.

4. BUNDLE STRESS MODEL DEVELOPMENT

4.1 FEM MODEL DEVELOPMENT WITH THE ANSYS CODE

The main objective in developing a Stress Model for CANDU fuel bundles was to be able to estimate stresses anywhere in the bundle given a defined bundle deformation. The CANDU fuel bundle is a complex mechanical structure. It is an array of parallel cylindrical fuel elements clad in Zircaloy-4 and secured to two endplates by resistance welds. As a structure, the CANDU fuel element is a thin cylindrical shell of Zircaloy-4 tubing which contains about 36 small cylindrical ceramic pellets of uranium dioxide. In unirradiated fuel, the pellets, however, do not fill the full axial length of the fuel element. A small radial gap of about 50 μm between the pellets and the cladding allows their axial movement.

On bending the fuel element, the pellets can readjust their positions until the cladding interferes with the pellets movement. The interference of the cladding with the pellets increases the fuel element stiffness and adds an additional stiffness to subsequent bending.

In the manufactured fuel element, the fuel cladding gap is filled with unpressurized Helium gas to help detect any defects in the manufactured of the fuel elements. On irradiation, the fuel pellets swell and the fuel elements deform. Fuel element deformation in a sinusoidal fashion is common. As a result, of these interactions, fuel pellet movement may be restricted following irradiation in a reactor.

The Bundle Stress Model of the CANDU fuel bundle was done for an unirradiated bundle. Model verification was accomplished by comparing predicted bundle deformations against those found experimentally for commercial non-irradiated CANDU fuel bundles.

In order to allow for variations in the simulation, the model was made parametric and written in ADPL (a Programming language) used in ANSYS. As a starting point for the FEM model, solid models of the CANDU fuel bundle components were developed with simplifications where justifiable to assist in reducing the modelling complexity. The FEM element mesh was then generated from the solid models with appropriate FEM modelling units using bricks or shells whenever appropriate. For instance, the fuel cladding used shell components for its FEM definition while the fuel pellets were constructed with brick type modules.

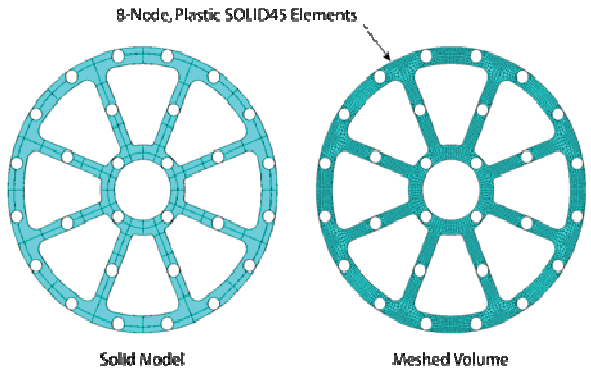

Figure 1: 28-Bundle Endplate

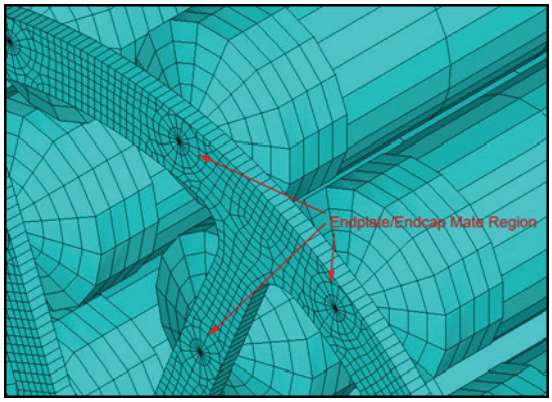

Figure 2: Detail of Bundle Endplate/ Endcaps FEM Mesh

An interesting interface occurs at the endplate/endcap region of the bundle where the endplate/endcap welds are located due to the various mating surfaces. In order to facilitate the numerical solution, the endcap shape was simplified and adjusted to contain the endplate weld and a portion of the endplate as a solid cylindrical appendage/spigot of length equal to the

thickness of the endplate. At the same time, the endplate was assumed to have circular through-the-wall perforations to mate with this cylindrical spigot of the endcap. By mating the endcap and endplate in this fashion, a smooth transition for the purpose of achieving a numerical solution was achieved. Figures 1 and 2 illustrate this particular part of the model.

Additionally, the CANDU fuel bundle has a number of appendages on the fuel cladding which are variously known as bearing pads and spacer pads. The bearing pads are on the outside of the bundle outer elements and serve the purpose of maintaining the bundle in a pre-determined distance from the pressure tube both for fluid flow effectiveness and bundle heat dissipation. The inner parts of the outer elements and the inner elements are provided with “spacer pads” to ensure the cladding of the fuel elements do not come into contact with each other and also to maintain appropriate spacing among the fuel elements to allow for fluid flow in the pressure tube.

The FEM model has also taken into account these minor details, albeit in a simplified form, whenever justifiable, to ensure that all contact points during the deformation of the bundle will be considered. Since the modelling is fully parametric, various models can be custom made for given bundle configurations, boundary conditions and deformations. This allows further exploration of the parameters of greatest sensitivity to the response of the bundles resulting in a better understanding of how the bundle responds to applied loads. A full view of the Bundle Stress Model finite element mesh for a 28-element CANDU fuel bundle is shown in Figure 3.

Tests to verify the Bundle Stress Model were conducted in an apparatus/rig designed for the purpose. The rig is able to hold a full size CANDU fuel bundle and capable of measuring bundle deformations when subjected to loads. The apparatus is illustrated in Figure 4 below.

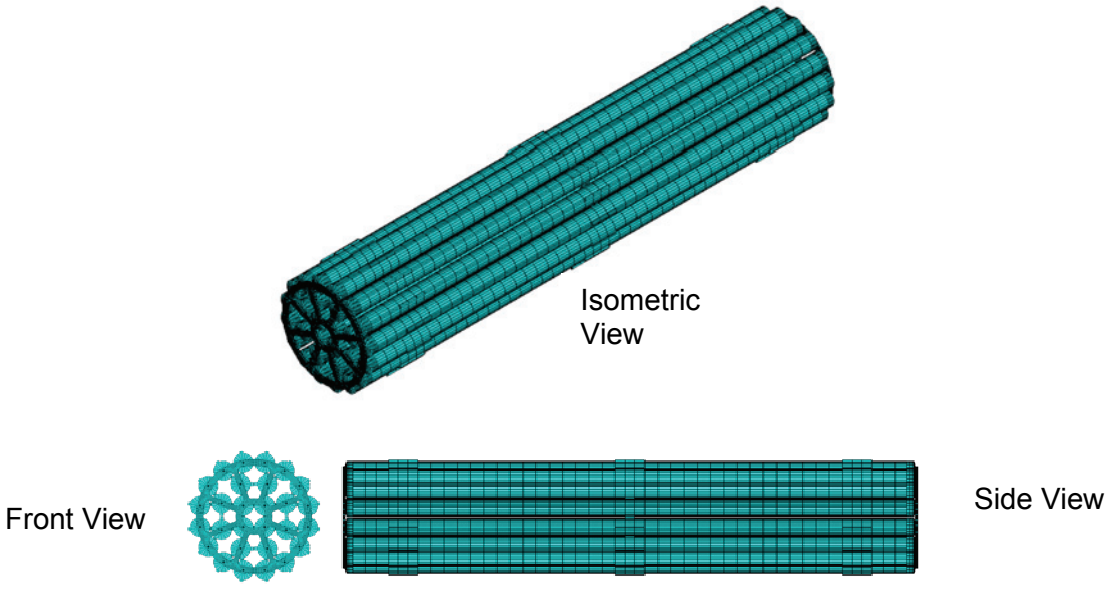

Figure 3: Finite Element Model of the 28- Element Pickering CANDU Fuel Bundle

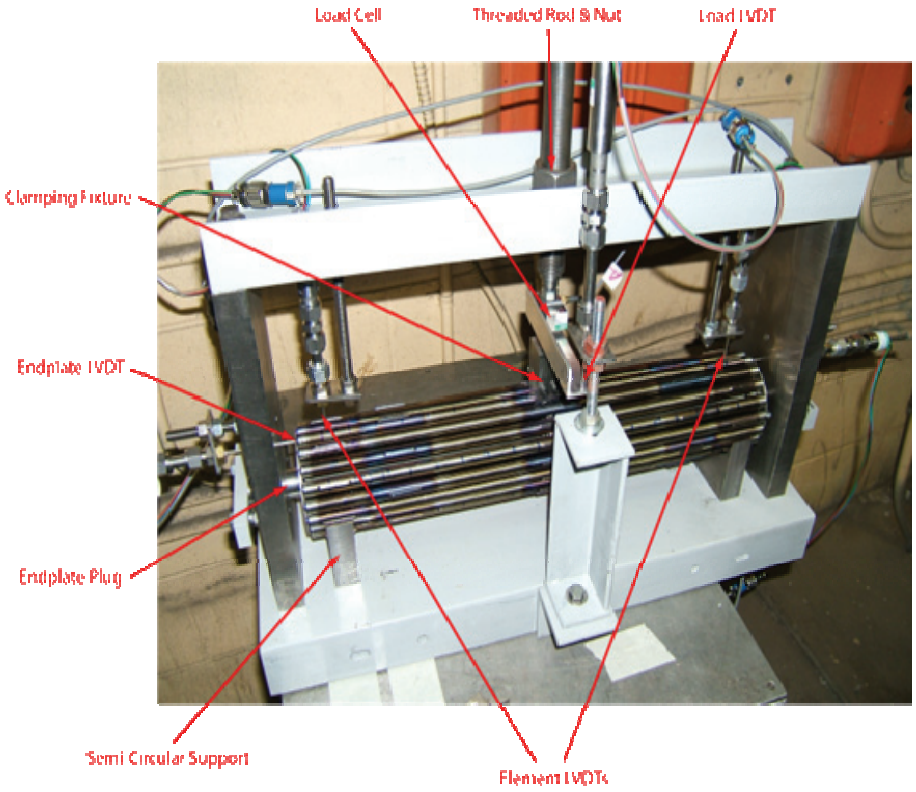

Figure 4: Test Apparatus Assembly

The deformations were measured at predetermined bundle locations by means of LVDT (Linear Differential Voltage Transducers). Three distinct types of loading were applied: “pull” loading where an outer element was pulled upwards and away from the bundle, “push” tests where an outer element was pushed in and a “bundle push” where about “five contiguous outer elements were pushed in simultaneously. In all cases, the bundle deformations were measured at the point of loading, near the bearing pads and at the two endplates.

The results were then compared with the simulations from the Bundle Stress Model for similar type of loading. The overall result from this verification of the model was the bundle model predicts the bundle to be less stiff than it actually is. That is, the model predicts larger deformations for a given load applied to an element than it actually occurs. At the same time, the endplates were found to behave stiffer than the Bundle Stress Model. However, notwithstanding the observed deviations, the model provides adequate results for loading deformations relevant to dry storage in the linear elastic regime.

The discrepancy between the test results and this early bundle stress model was suspected to be due to the approach taking to model the pellets within the fuel cladding as connected rigid bodies. The point of contact between the fuel cladding and the pellet-to-pellet contact were modelled as rigid mechanical structures. In the next iteration of the Bundle Stress Model development, this was taken into account as it will be described in the next section.

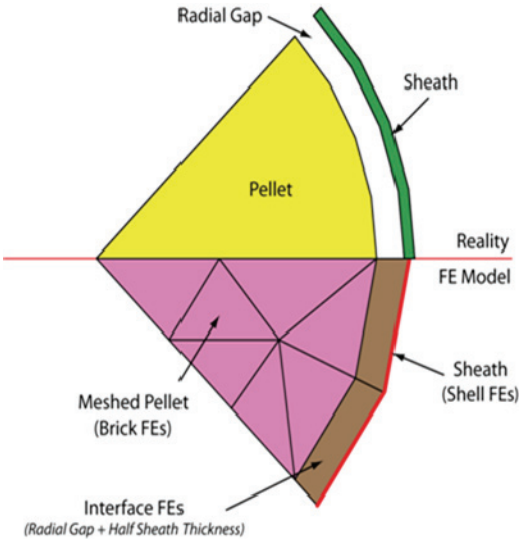

Figure 5: Pellet-to-Sheath Contact

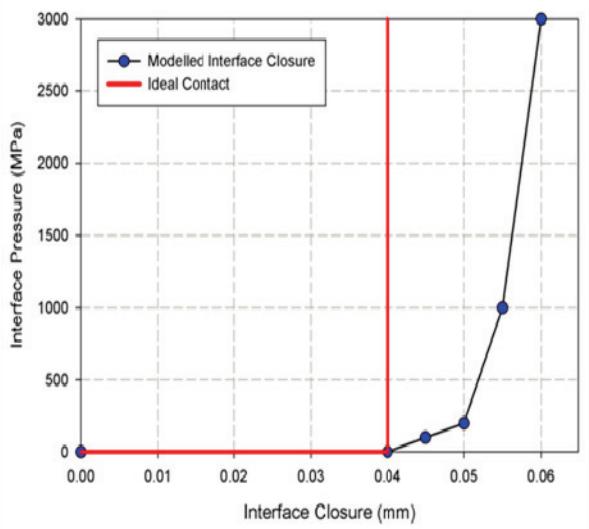

Figure 6: Pellet-to-Sheath Interface Material Properties

4.2 IMPROVED BUNDLE STRESS MODEL WITH INTERFACE FINITE ELEMENT

Initial fuel element models treated the fuel pellets and the cladding as distinct geometrical objects. Contact between the pellets and the sheath were modelled using the standard contact analysis approach in ANSYS. However, the geometrical discontinuities between the pellets and the cladding greatly affected the convergence and stability of the model.

In the new approach, the fuel element is treated as a continuous solid object. Contacts between pellets and cladding are modelled using a continuous material interface (see Figure 5) with the capability of transmitting compressive forces normal to mating surfaces such as the pellet and the cladding.

Figure 6 illustrates the material behaviour at the interface provided by the interface finite element. Until the pellet and cladding surfaces contact each other there are no normal stresses. When the radial gap between the pellet and cladding surface is closed (0.04 mm in Figure 6), contact takes place and the normal stresses at the interface become non-zero. The value of the equilibrium normal stresses between the mating surfaces is unknown, but it was found through analysis that the maximum equilibrium stress normal to the sheath mid-surface peaked at about 8 MPa for high non-axial loads. This stress is relatively small, so that equilibrium is achieved at small normal stresses. However, the finite element solver requires higher normal stresses to reach convergence and, for this reason, the material properties shown in Figure 6 have been extended to higher deformations and normal stresses or pressures.

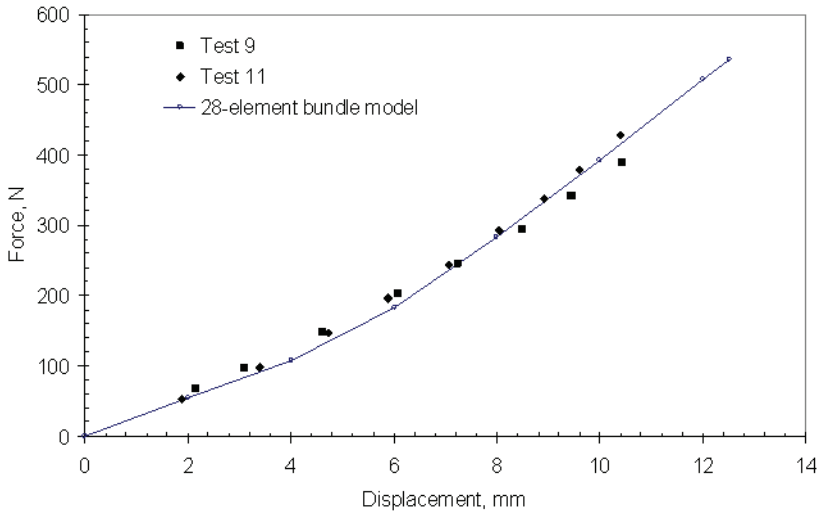

Figure 7: Measured and Modelled Response of 28-Element CANDU Fuel Element

The development of other modelling components such as the endcaps, bearing and spacer pads are similar to the previous models (Lampman et al., 2009). The pellet-to-pellet interaction was modelled using a combination of surface contact paired finite elements (TARGET170 and CONTACT173 in ANSYS). Each contact pair is modelled with a different real constant in order to monitor and model the gaps between all the pellets. The axial gap between pellets is not modelled geometrically but through a contact offset value declared for each contact pair. In practice, the axial gap between pellets varies but an average axial separation between the pellets of 0.02 mm was chosen following a sensitivity study of various key parameters affecting the model including pellet-to-pellet contact and axial pellet-to-pellet separation.

4.2.1 Validation of the Modified Fuel Element Model

The new fuel element model was used to simulate the test results obtained for the 28-element CANDU fuel bundle single fuel element (see Figure 7). The experimental test conditions were simulated in great detail. Regions of the endplate that were clamped by the test apparatus were modelled by suppressing node movements in all directions. The material properties and dimensions of the single fuel element including the pellets sizes followed the fuel element design description.

Displacements of 2, 4, 6, 10, 12 and 12.5 mm were applied to the model at the middle bearing pad to coincide with the location of the middle LVDT (Linear Voltage Differential Transducer). The resulting forces at the bearing pad nodes obtained through the model were then summed up to obtain the total reaction force which corresponds with the load that would have been applied to the single element in a similar test.

Calculated forces and displacements obtained from the model were then compared with the test results. The comparison is shown in figure 7. The agreement between experimental and

simulated values from the new single element fuel element model is very good. It is of particular interest to note that the new fuel element model with interface finite elements between the pellets and the cladding correctly predicts the fuel element stiffening at the higher loads under plastic deformation.

5. DELAYED HYDRIDE CRACKING (DHC) PROGRAM

The purpose of the Delayed Hydride Cracking (DHC) Program was to complement the Bundle Stress Model development by providing fundamental material properties data that could be used for assessing the susceptibility of the CANDU fuel bundle endplate/endcap welds to the phenomenon of DHC. In order to establish whether DHC is operative at the endplate welds during dry storage, material properties such as the stress intensity factor (K_{IH}) for DHC initiation and delayed hydride crack velocity (DHCV) are required.

A test apparatus was developed for performing delayed hydride cracking (DHC) tests on the assembly fuel element welds of a fuel bundle. Experimental procedures to measure the stress intensity factor (K_{IH}) for DHC initiation from the weld and the crack velocity (DHCV) were also developed. A finite-element stress analysis methodology was also developed to calculate the applied stress intensity factor at the weld discontinuity under the loading conditions of the experiment. A test apparatus, test procedure and stress analysis methodology were developed and used to determine the K_{IH} and DHCV of the endplate welds from two General Electric (GE) 37-element unirradiated fuel bundles in 2008 (Shek and Wasiluk, 2009).

5.1 DEVELOPMENT OF TEST APPARATUS AND TEST METHODOLOGY

A schematic view of the apparatus devised for testing of endplate/endcap fuel bundle welds under conditions relevant to the dry storage of the fuel is shown in Figure 8. It illustrates its basic components which include a loading rig, furnace for heating, crack monitoring system using both acoustic emission and direct current potential drop, and data acquisition and control system. The loading rig uses a cantilever type of test. Two different arrangements for providing a load on the test specimen are shown in figure 9. On the left rig, the load pulls on the test specimen upwards while on the right rig, the load pulls downwards. Both rigs were designed to operate in a hot-cell to test irradiated fuel endplate/endcap welds, however, all the bundles tested in the program were unirradiated.

The sample specimen tested consisted of a portion of an empty fuel element (i.e. without fuel pellets) with a part of its endplate still attached. The test is performed by holding the endplate portion firmly secured between two purposely custom designed SS solid blocks and applying a load on the fuel element end, hence acting as a cantilever. The torque thus provided acts on the weld and provides the required energy to fracture the weld. The majority of the tests were done at 150^{o}C which is the nominal maximum fuel temperature that could be expected during dry storage of CANDU fuel in the DSCs, the actual temperature being significantly less.

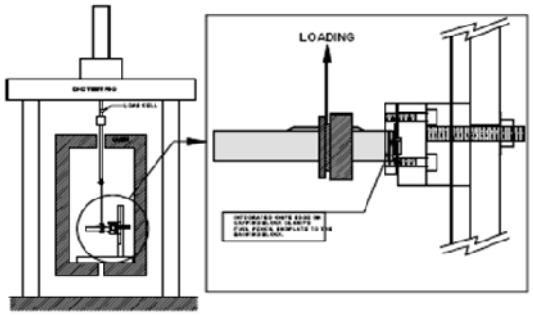

Figure 8: Schematic of Test Apparatus showing the Loading Arrangement

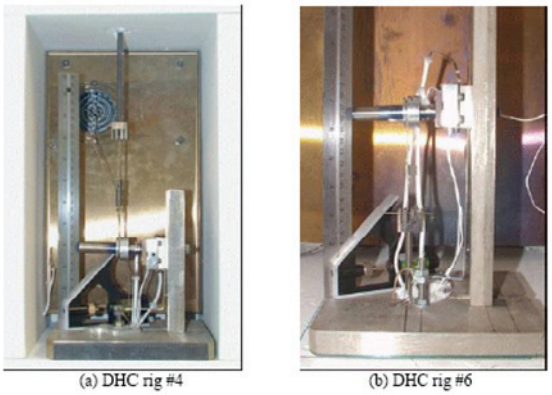

Figure 9: Detail of Loading Arrangement

Figure 8 shows that the sample is loaded by pulling up on the fuel element through a steel cable placed around a groove in an aluminum collar attached to the fuel element. This produces a tensile bending stress in the lower part of the weld. The pull rod is connected to a load cell and an actuator, controlled by a stepper-motor. The loading system is designed with a relatively short lever arm (e.g. 28.68 mm in the illustration shown in Figure 9) to avoid having a large bending moment at the weld. As shown in Figure 9, the loading system can be designed to pull down on the fuel element, in which case the top part of the weld will be under tensile bending stress.

Heating is provided by a furnace with a programmable temperature controller. The allowable temperature fluctuation in the isothermal K_{IH} or DHCV tests is ± 2ºC from the target temperature. Crack initiation and growth is monitored by acoustic emission and direct current potential drop techniques simultaneously. A wave guide is used to transmit the acoustic emission signals to the transducer outside of the oven. For the potential drop crack detection and monitoring system, microvolt resolution is required to detect cracking. A constant current of 3-4 amperes was used in the D.C. potential drop (PD) monitoring. The acoustic emission system is capable of detecting the breaking of a 0.5 mm H pencil lead when the background noise is low. It should be pointed out that the test procedure is designed to have continued crack growth after initiation, which would be easier to detect than just crack initiation.

The CANDU fuel bundles used in the tests were manufactured without UO_2 pellets. They were prepared for testing by first hydriding them to a specified hydrogen concentration of 40 ppm by the electrolytic/thermal diffusion hydriding technique. After electrolytic hydriding, a 75 mm long portion of the bundle was sectioned off by wire electrical discharge machining. For the tests, a portion of a single element with a portion of the endplate attached was used. The endplate attached to the single element was firmly secured to the test apparatus and then a load was applied incrementally to the fuel element at about 75 mm away from the endplate. The torque produced acted on the endplate/endcap weld and led to its cracking after a critical load was reached.

The loading process was followed by monitoring the voltage differential across the crack. After cracking initiated, the voltage differential began to increase steadily in a linear fashion. The rate of the voltage differential increase over time allowed the estimation of the velocity of cracking.

After a sufficient growth of the crack was achieved, the process of cracking was arrested by elevating the temperature by 50°C above the test temperature for a short time interval. This stopped the cracking of the specimen since the hydrides at the tip re-dissolved. While the cracking is stopped, tinting of the fractured surfaces of the crack by oxidation is done. The tint is used for measuring the length of the fracture. Since the time elapsed for crack initiation to crack arrest can be determined from the experiment, the crack velocity can be estimated. After tinting, the test specimen was brought back to the original test temperature and the testing resumed. As it is characteristic of DHC, the cracking continued shortly thereafter but the velocity of cracking after the tinting was observed to be higher than in the first period prior to tinting.

The apparatus was verified by testing endplate/endcap welds from a commercial GE bundle. The results of this testing indicated that the developed apparatus performs as designed. Weld morphology examination through SEM also confirmed that the cracking of the endplate/endcap welds tested with the apparatus was Delayed Hydride Cracking or DHC.

5.2 CALCULATED STRESS INTENSITY FACTORS (ANALYTICAL AND FEM MODEL)

5.2.1 Profile of Weld Discontinuity

In order to calculate the K_I at the weld discontinuity, which is treated as an initiating crack, the depth and profile of the weld discontinuity has to be determined. This is done by metallographic examination (and/or fractography) of the weld to determine the dimensions of the notch and weld discontinuity. Figure 10 is a metallographic section of the weld prepared after a K_{IH} test). The depth of the notch formed between the endplate and the endcap, and, the depth of the weld discontinuity can be measured from the metallographic section. These parameters are then used as input to calculate the applied K_I in the DHC test.

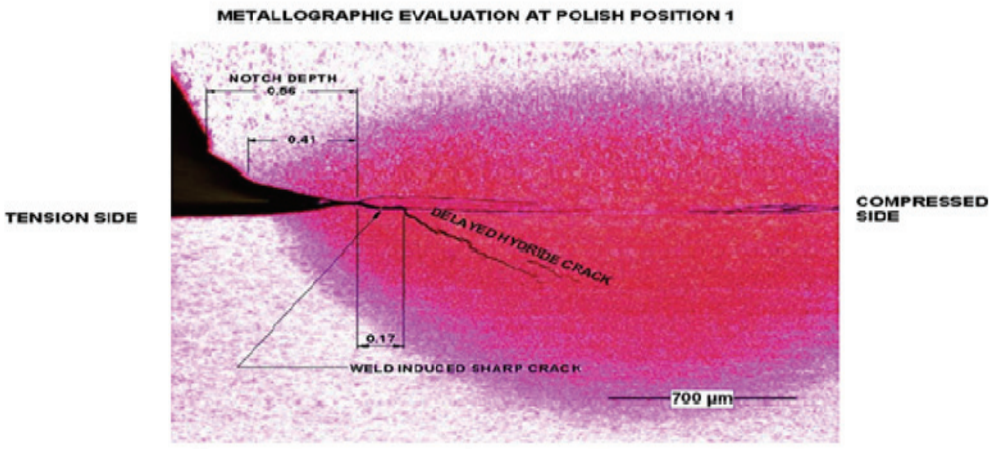

Figure 10: Metallographic Section of Sample Showing the Weld Notch. Weld Discontinuity and DHC Crack (Test 07-09)

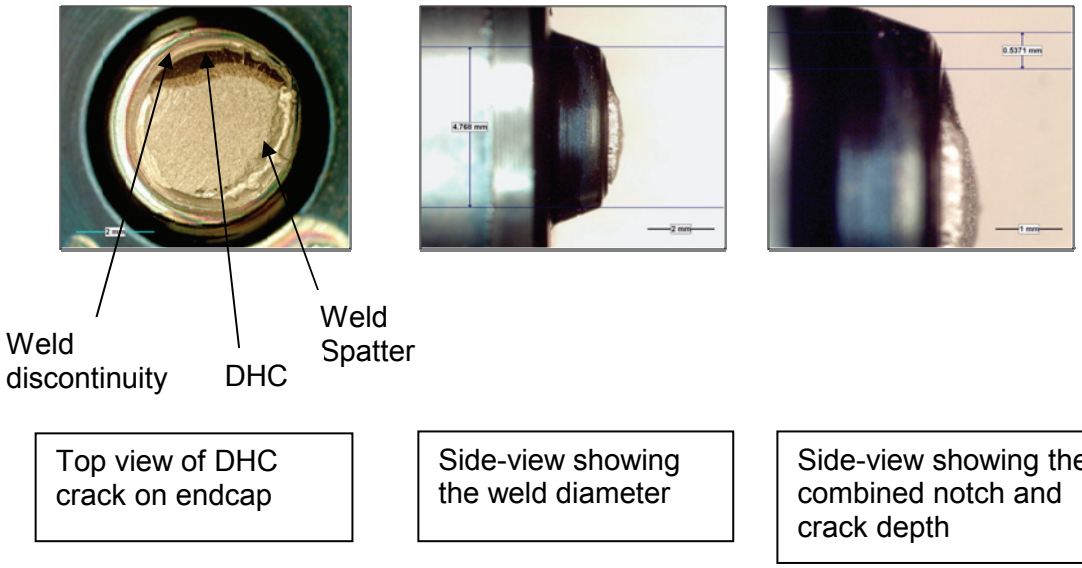

Figure 11: Fracture Surface on the Endcap after the DHC Test to Illustrate the Appearance of the Weld Discontinuity and Weld Spatter (Commissioning Test 07-104)

Figure 11 shows an example of a DHC crack of the apparatus commissioning test. The diameter of the weld and the combined depth of the notch and weld discontinuity can be determined from the side-view of the fracture surface. Figure 11 also shows the presence of weld spatter on the endcap surface. However, the spatter does not appear to affect the depth of the notch and weld discontinuity or the load-bearing area.

5.2.2 Development of Stress Analysis Methodology

The Stress Intensity factors (K_I) at the weld discontinuities of the welds tested in the DHC experimental program were calculated using both analytical and finite element analyses. In the analytical analysis, the sample was modeled as a cantilever rod with a fully circumferential crack. Two solutions for K_I available from the open literature were used: The Erdogan and Tada method (I) and the Benthem Method (II).

For the finite element analysis, two approaches were used for each model:

1. In a simplified approach (model “a”), boundary conditions which constrain displacement in the axial direction but allow fuel element and weld ovalization, were applied at the end of the element.
2. In a more detailed approach (model “b”), the boundary conditions included the endplate at the end of the fuel element. Since the analysis is linear-elastic, local deformation of the fuel element shell under the applied load would not affect the KI value.

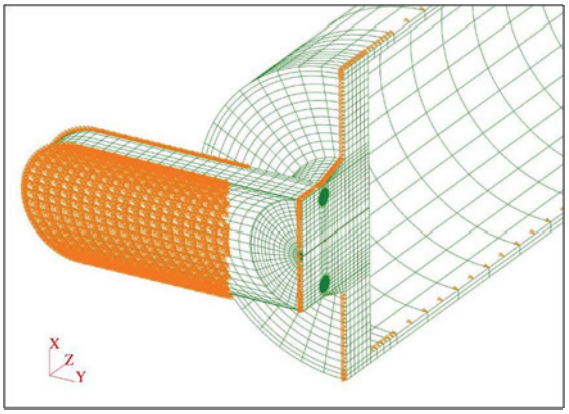

Figure 12: Finite Element Model of a Fuel Bundle Element with a Circumferential Crack (Model III-b)

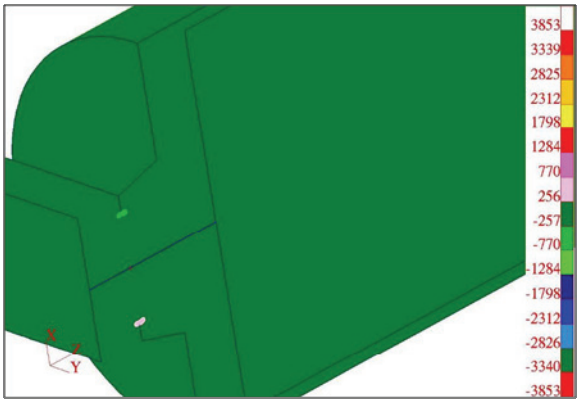

Figure 13: Opening/Closing Stress Component (MPa) (Model III-b)

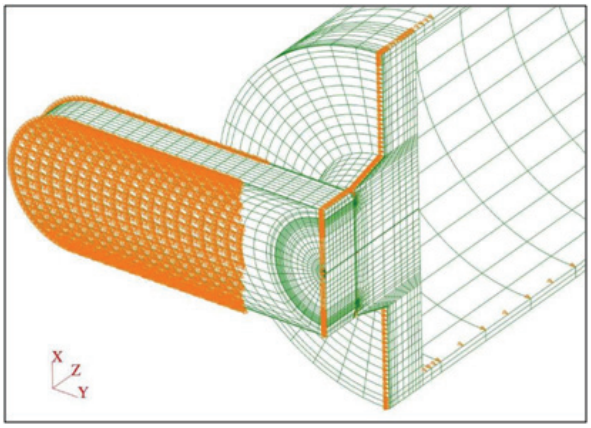

Figure 14: Finite Element Model of a Fuel Bundle Element with a Circumferential Crack (Model IV-b)

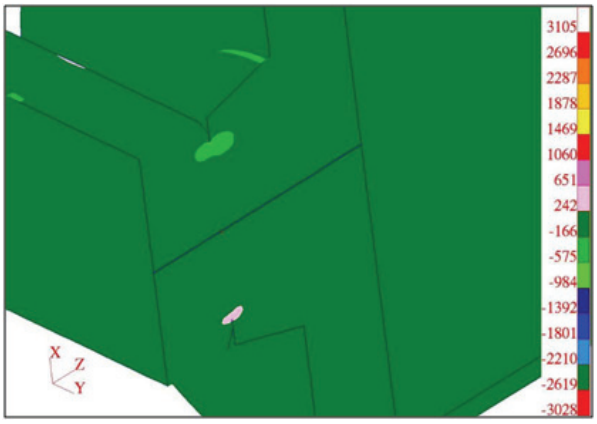

Figure 15: Opening/Closing Stress Component (MPa) (Model IV-b)

The finite element modeling, however, does not consider crack closure caused by the compressive bending stress that occurs in the lower portion of the specimen. The crack closure, if present, would increase the load carrying capacity of the component and hence decrease the applied effective tensile stress.

In both approaches, four levels of complexity (Model I to IV) representing higher levels of detail to the actual tests were modelled. Model I analyzed a circumferential crack in a rod. Model II analyzed a circumferential crack in an endcap with uniform diameter. Model III analyzed a circumferential crack in an endcap with geometry closer to that of the actual sample (having a tapered portion). Model IV analyzed the circumferential crack at the root of a notch which is the closest to the actual sample geometry. Both models III-b and IV-b are illustrated in figures 12 to 15.

Table 2: Stress Intensity Factors from Analytical Approach

Solution	K_I [MPa√m]
Method I (Erdogan and Tada)	10.0
Method II (Benthem)	10.4

The stress intensity factor for a GE-37 element bundle weld tested for K_{IH} at 130°C (07_09 test) as part of the commissioning of the test apparatus, was computed using the analytical approach and is documented in Table 2. Benthem et al. (1972) solution produced higher stress intensity factors than Erdogan (1982) and Tada et al. (1985) solutions.

Table 3: Crack Driving Force from Numerical Approach

FE Model	J [N/mm]	K_I [MPa√m]
Model I-a	0.887	10.0
Model I-b	0.538	7.8
Model II-a	0.893	10.0
Model II-b	0.543	7.8
Model III-a	0.962	10.4
Model IV-a	0.962	10.4
Model IV-b	0.575	8.0

Table 3 above presents computed crack driving forces from finite element models in terms of stress intensity factors and J-integrals as well as the corresponding stress intensity factors. The highest stress intensity factor was 10.4 MPa√m obtained from Models III-a, and, IV-a. The lowest stress intensity factor, 7.8 MPa√m, was computed from Models I-b and II-b. The maximum difference in the computed stress intensity factors was 2.6 MPa√m. However, if only results from type 'a' or 'b' models are compared, then this difference is considerably smaller. The general trend is that the stress intensity factors from type 'a' models were higher than from type 'b' models. Since type 'b' models were more detailed and closer to the experimental setup, they were used to determine the applied K_I in the experiments. Another observation is that stress intensity factors computed from Models III and IV type are quite similar.

5.2.3 Canadian Commercial CANDU Fuel Bundles DHC Database

After the successful development of the test apparatus for Delayed Hydride Cracking of the CANDU fuel bundle endplate/endcap welds, the preliminary database from that effort was expanded to include other fuel bundles types and manufacturers. In the preliminary database, the endplate welds from two General Electric (GE) 37-element unirradiated fuel bundles were tested in 2008 (Shek and Wasiluk, 2009). A total of five endplate welds were tested at 130°C and 150°C and the K_{IH} values of four welds ranged from 7.6 to 8.3 MPa√m. The other sample had a K_{IH} value of 13.6 MPa√m.

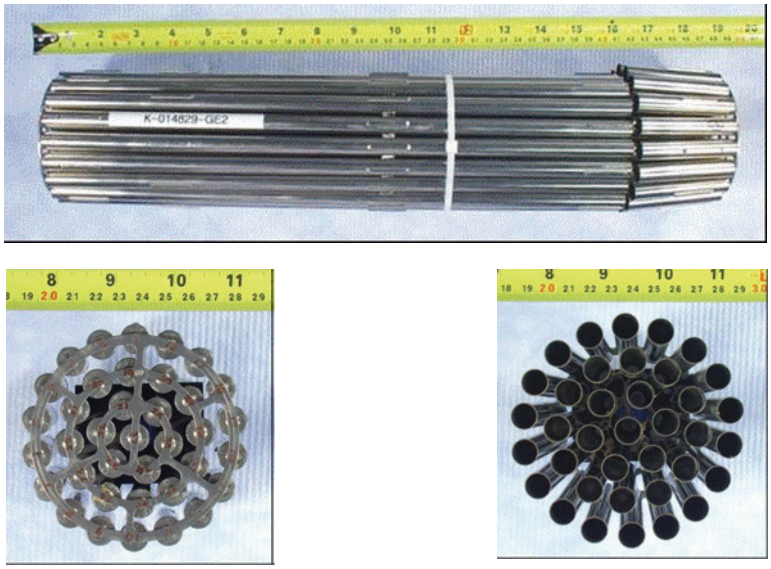

Figure 16: The empty fuel bundle elements - see right end of the bundle – sprung out after being sawn off.

In the additional tests, three empty unirradiated fuel bundles without the fuel pellets inside the fuel elements were used: one GE 28-element bundle, one GE 37-element bundle and one CAMECO 37-element bundle. These empty fuel bundles were made using standard manufacturing and welding processes and they did not have a serial number. Results of the DHC tests are given in the next chapter.

After electrolytic hydriding, a 75 mm long portion of the bundle was saw-off by wire electrical discharge machining from the three bundles (Figure 16). It was noted that the fuel elements in all three end sawed-off bundle portions sprung out after cutting, likely due to the presence of residual stresses in the endplate assembly.

The three sawed-off end portions of the bundles were placed in a large oven and annealed at 266°C for 47 hours in order to diffuse the hydrogen from the surface hydride layer into the bulk metal to obtain a target hydrogen concentration of 40 ppm. It was noted that the CAMECO bundle had a different oxide colour than the GE bundles after the diffusion anneal.

A coupon was taken from the endplate weld of each bundle for hydrogen concentration measurements. The remnant of the hydride layer on the coupon was removed by pickling and

grinding. The Terminal Solid Solubility for hydride dissolution (TSSD) temperature of each coupon was measured by differential scanning calorimetry. The coupons were then sent to Nu-Tech to measure the hydrogen concentration by hot extraction inert gas fusion analysis using a LECO instrument.

The TSSD temperatures ranged from 283°C to 288°C, which are higher than the TSSD temperature of 270°C measured from the endplate weld of the hydrided bundle tested in 2008 (Shek and Wasiluk, 2009). The measured hydrogen concentrations ranged from 55-61 ppm which was higher than the targeted concentration of 40 ppm. This is acceptable as the DHC properties at the designed test temperature of 150°C would not be affected by the higher hydrogen concentration. The remnant of the hydride layer was left on the bundles.

6. RESULTS OF THE USED FUEL INTEGRITY PROGRAM

As indicated earlier, the thrust of the used fuel integrity program is to provide assurance that the fuel stored in long-term dry storage will not undergo degradation that could compromise its future transfer from dry storage to a Deep Geological Repository or DGR. The results of the program indicate that CANDU fuel will be able to be handled and transported from dry storage without adverse impact from its long term storage in the Dry Storage Containers (DSC's).

6.1 STRESS FIELDS PREDICTIONS WITH THE BUNDLE STRESS MODEL

In validating the Bundle Stress Model, a number of mechanical tests were made on full size commercial 28- and 37- element bundles. The tests consisted in applying loads to the bundles in a pre-set location at the middle of the bundle and then measuring the bundle deformation. When, an outer element of the bundle was pulled, the displacements of the bundles at specific locations such at the point of load application and the endplates were compared with the values predicted by the model. The applied loads were intended to cover bundle deformations in both the elastic and plastic regimes. This was done to test the robustness of the modelling since deformations of the bundles while in dry storage are not expected to be beyond the elastic regime.

The discussion will concentrate on the pull tests performed on the Pickering 28- element bundle manufactured by General Electric Inc. since results from the 37 element bundle and tests other than pull tests were similar. Three "pull" tests were performed on the 28-element bundle with loads ranging from 0-400N performed in increments of 20N and 50N.

The *pull test* involved pulling a single element at its midpoint in a radial direction away from the bundle central axis while constraining the bundle endplate. Both the displacement and load at the point where the load is applied are recorded. Displacement measurements were also made at other locations in the fuel element near the endplates and at the endplates.

Results of these tests are summarized graphically below for 28-element Pickering type bundles (see figures 17 to 22). Similar results were also found for Bruce type bundles. The results illustrate the bundle behaviour when an outer element is pulled with increasing larger loads.

28-Element CANDU Fuel Bundle Pull Test– Test and Simulation Results

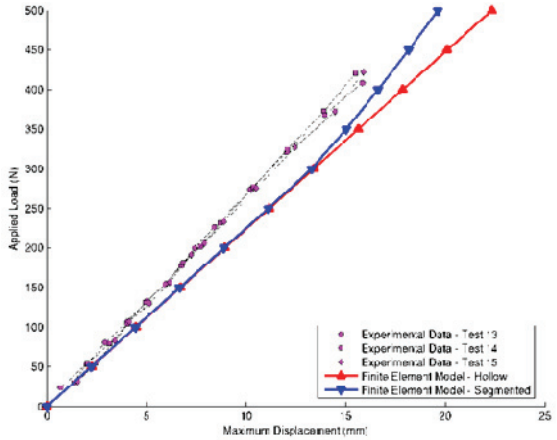

Figure 17: Load LVDT Displacement

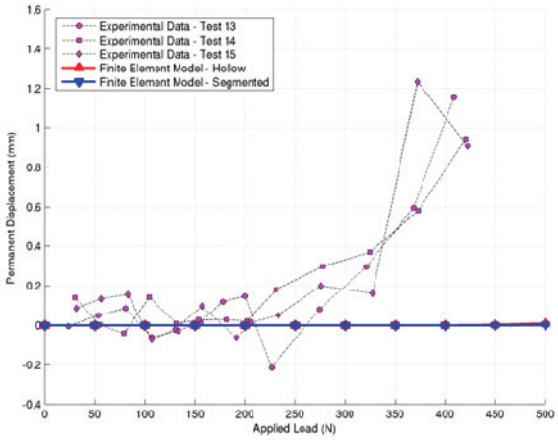

Figure 18: Load LVDT Plasticity

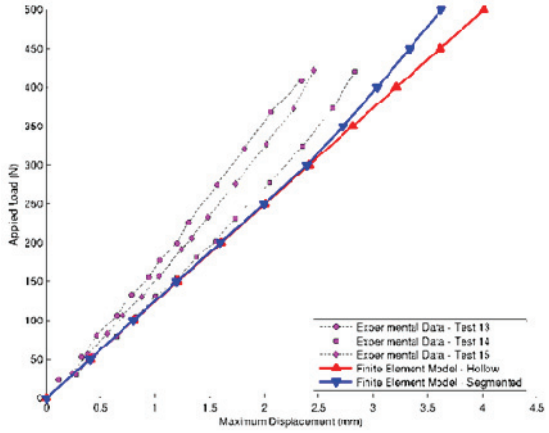

Figure 19: Left Element LVDT Displacement

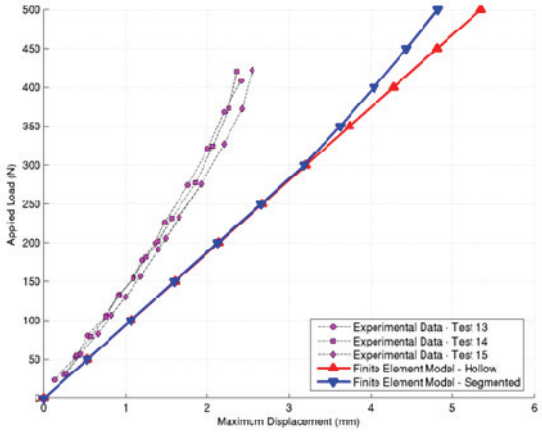

Figure 20: Right Element LVDT Displacement

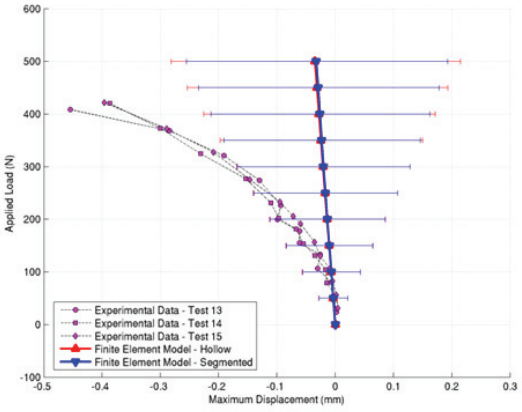

Figure 21: Left Endplate LVDT Displacement

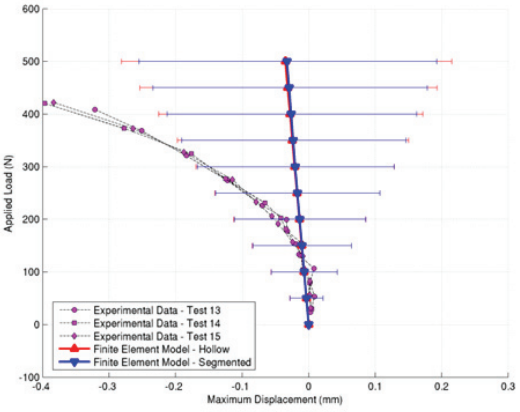

Figure 22: Right Endplate LVDT Displacement

The simulation model over predicts the observed displacements by about 20% at the centre of the pulled element (Fig. 17), and, by about 25% at the location of the left LVDT (30 mm from the left endplate (Fig.19). However, displacements 37 mm from the right endplate (Fig. 20) are about twice as large as those found experimentally. Additionally, the simulation results from the hollow bundle model predict the bundle should behave elastically for the whole range of loads up to 400 N applied to the bundle (Figs. 17, 19 and 20), and this is also indicated by the plot of permanent displacements shown in Fig. 16. However, both the experimental results of Fig. 17 and the bundle behaviour shown in figure 18 indicate that the bundle begins to behave plastically for loads greater than about 200 N.

At applied forces less than approximately 300 N, there is no observable difference between the hollow and segmented pellet models. However, as applied loads exceed 300 N, the pellets act to stiffen the elements. This also appears to be observed in some of the experimental results primarily the values from the right end LVDT (fig. 18). In general, more displacement was seen along the element in the simulations than in the experiments. At applied loads less than 50 N the modelled and experimental results agree within the experimental uncertainty, but the slope of the lines up to the plastic region, between 200 N and 300 N applied force from the experimental data, suggests the modelled elements are not sufficiently stiff.

The results for the modelled endplate LVDT data contain “error bars” associated with the values (Figs. 21 and 22). The plotted values are based on the displacements of the endplate at the element axis, but in the experiments the LVDT does not measure this displacement exactly. The error bars are plotted to indicate the range of possible displacements of the LVDT in the weld region.

Comparison of the endplate LVDT displacements shows that the modelled endplates are stiffer than those observed in the experiment. At low applied load, the results may be the same given the large uncertainty of the measurement based on LVDT position, but at higher load the endplate behaves very differently between the model and the experiment.

The permanent displacement for the LVDT at the load point of application per load cycle is plotted against the experimental data in Fig. 16. Displacements at other locations of the bundle follow similar trends. From the experimental data, permanent deformation of the element is first observable in the range between 200 N to 300 N. However, the modelled results show no indication of significant plastic deformation.

The hollow model predicts a linear relationship between load and displacement for the whole range of loads tested consistent with linear elastic behaviour. Similarly, the experimentally found displacement values at the centre of the pulled element and towards the left endplate also behaved linearly, except for the displacements recorded near the right endplate. Since the experimental results are observed to be quite repeatable and provide consistent results, the observed bundle behaviour cannot be readily explained as a result of experimental error. Rather, it would appear to indicate that the bundle characteristics have an in-built asymmetry.

This asymmetric behaviour could well be caused by material properties dissimilarities at the endplate/endcap welds. Since the endplate/endcap welds were treated as having the same properties as Zircaloy-4, the results could indicate that this assumption should be more fully explored. Additionally, over time, the fabrication of Zircaloy-4 has changed and it is also possible that the Zircaloy-4 produced for the test bundles has an elastic modulus that drifted significantly from the Zircaloy-4 used to generate the MATPRO data. It is clear from the pull

test results that the plastic material properties given in MATPRO might not be reliable for mechanical modelling of the CANDU fuel bundle.

The segmented model that includes the pellets reduces the simulated bundle displacement towards the experimentally observed values but it does not quite explain the observed behaviour, either. It is observed that the segmented pellet model also provides a linear relationship between load and displacement consistent with linear elastic behaviour. While addition of the pellets to the model does approach the general behaviour of the observed displacements near the endplates, it fails to predict the behaviour observed for displacements at the point of application of the load. Even though, the new predicted values from the simulation are closer to the observed values and reduce the variance between observed and predicted displacements at the mid-point of the pulled element to about 10%.

Typical results for the 28-element bundle are shown in figures 17 to 22. The applied load is plotted against the maximum displacement measured for each of the LVDTs. The plotted simulation results also include simulation results from the hollow element bundle stress model along with the segmented pellet model to indicate what extent pellets effects are important.

Two other types of tests have also been investigated: *element push test* where the outer bearing pad of an element is pushed radially inward into the bundle, and, a *center load test* which involves pushing the entire bundle at its center and measuring its displacement. The results are similar to the pull tests and indicate similar discrepancies between the model and data from the experimental tests.

As indicated earlier, forces applied to the bundles during storage or transportation are normally at the low end of the applied forces used in these tests, and, unlikely to be greater than 100 N. In this range, the model provides an adequate tool to predict stresses in the bundle relevant to its management. An attempt to address the observed discrepancies by modifying the bundle stress model was done and the details of this effort have been described earlier in section 4.2. The new approach to the modelling included freeing the constraints on the pellets but including a fictitious finite element between the pellets and the cladding to transmit forces acting normal between the pellet and the inner wall of the clad as a result of the fuel cladding interference with the non-deformable pellet as the bending of the element proceeds as a result of the force acting on the element such as a pull force during the pull tests. This modification to the model provided excellent agreement with the displacement values obtained in the tests. A comparison of the results of the simulation and the data is illustrated in figure 7 above in section 4.2.

6.2 STRESS INTENSITY FACTORS AT THE ENDPLATE/ENDCAP WELDS

The developed finite element CANDU fuel bundle models were described earlier (see section 4). Finite element sub-models were also developed to more accurately model the assembly weld regions of a bundle. A weld crack was included in the sub-models and a special mesh generated to allow for the calculation of stress intensity factors. Since the weld notch in the endplate/endcap welds is very sharp, the notch was conservatively modeled as a crack in the finite element sub-model.

Fuel bundles, stored in the Dry Storage Containers or DSCs, are transferred to the DSC from the waterpool in their waterpool storage modules. During the transfer, the fuel is vacuum dried. The storage module has an array of thin shell stainless steel cylindrical tubes of 105 mm

diameter where the fuel bundles are stored in a horizontal position. As a result, the fuel bundles are supported by the module tube and no axial forces are applied to them.

The fuel bundles temperature steadily decreases during dry storage as the heat of decay of the fuel decreases. Since the DSCs are stored in an unheated storage facility, the diurnal and seasonal temperature changes of the ambient temperature of the facility also affect the bundles storage temperature resulting in minor fluctuations of the mean fuel storage temperature. At the start of dry storage, the expected temperature of the fuel is about 130°C. The initiation of Delayed Hydride Cracking is expected to be relatively insensitive to temperature, but the velocity of crack propagation increases with temperature. If DHC is active in dry storage, then crack growth is expected to initiate at the start of storage. Consequently, the initial dry storage temperature of 130°C was used for this analysis.

In-reactor, the bundle experiences significant mechanical loadings due to the presence of the other bundles in the pressure tube, the coolant fluid flow, and, the irradiation process itself. As a result, distortions to the bundle original geometry occur and can be measured by profilometry from Post Irradiation Examinations (PIE). Based on these examinations, a number of typical bundle geometry deformations were modeled with the Bundle Stress Model to obtain an estimate of the range of stress fields that could be expected in the fuel bundle endplate/endcap region during dry storage. These stress fields were then used as an input to the FEM sub-models of the endplate/endcap region in order to calculate the stress intensity factors (KI values) at the assembly weld cracks. The estimated KI values were then compared against experimentally found critical stress intensity factors for DHC activation. In this way, an assessment can be made as to whether Delayed Hydride Cracking of the endplate/endcap welds is operative during the bundles dry storage.

The following key aspects of the fuel bundle models were varied for the stress intensity factors calculations:

1. material properties to account for the effects of irradiation and temperature;

2. fuel element bowing in the plane perpendicular to the bundle axis to account for post-reactor discharge bundle geometry; and

3. fuel element models to account for the effect of fuel pellet interactions with the fuel element sheath and adjacent pellets.

Additionally, full advantage was taken of the several fuel bundle model variations that were developed to simplify the calculation process whenever it was feasible. This is accomplished by judiciously implementing in the fuel bundle model a combination of any of the following four fuel element sub-models: a *pipe model using* pipe finite elements to model the sheath and the mass of the pellets; a *hollow model with* the sheath explicitly modelled using shell finite elements and with the mass of the pellets included; a *pellet contact model*, which is an extension of the hollow model with individual pellets and pellet-to-pellet and pellet-to-sheath contacts modelled using contact and target surfaces; and the *pellet interface model* with individual pellets and the pellet-to-pellet and pellet-to-sheath contacts modelled using interface finite elements.

The fuel bundle finite element models (Lampman *et al.*, 2009; Popescu and Lampman, 2009) for the simulation of the 28-element fuel bundle have between 300,000 and 500,000 degrees of freedom, depending on the options chosen for the pellet-to-sheath interaction. A steady-state

solution is found, however, 3 to 10 iterations are usually needed to solve the geometrical non-linearities, *i.e.* to solve the fuel element components (sheath and pellets) interface contacts. Further, the sub-models to calculate the stress intensity factor at the assembly welds have more than 200,000 degrees of freedom.

During in-reactor irradiation, the fuel bundle pellets crack, and, their dimensions change. The extent of cracking and dimensional change depends on the fuel element power history. Measurements of irradiated pellet diameter have been made during PIE. However, because of pellet cracking and relocation, the measurements are not sufficiently accurate for modelling purposes.

Experience from PIE is that the fuel pellets cannot be easily removed from irradiated fuel elements without force. This would indicate that the gaps between the fuel pellets and the sheath are smaller than those in the original non-irradiated fuel element. This observation on the effect of irradiation on the fuel element was simulated by selecting virtually closed axial and radial pellet gaps. From each of the simulations, the maximum displacement of the central bearing pad on element 5 relative to the endplate was determined for comparison of the fuel element deformation. As well, the 28-element sub-model of the assembly weld region was used to determine the maximum K_I value at the weld crack tip.

Since the selection of a fuel element model may have a significant impact on the response of the fuel bundle, a conservative approach regarding the fuel element model was followed. The hollow element being without fuel pellets is less stiff than one that has the pellets, and, as a result, it would also show the largest degree of bending for a given load resulting in the largest K_I value. To confirm this expectation, a comparison of the irradiated hollow fuel element model and the irradiated interface model under identical loads and boundary conditions was performed using for the comparison, the full 28-element fuel bundle model.

ANSYS 11.0 was used to solve the model with the two different fuel element models. All simulations were performed with irradiated material properties at a temperature of 130°C. The hollow fuel element model simulation used the best fit geometry determined from the unirradiated sensitivity studies (Popescu and Lampman, 2009). The irradiated interface element model also used the best-fit geometry with the exception that reduced pellet gaps were modelled to represent the effect irradiation appears to have on the fuel element response. Results of these simulations are shown in Table 4 below.

The interface model with near closure of the pellet gaps gives significantly less deflection of the element and a lower K_I value at the assembly weld. Because of the uncertainty in the irradiated fuel element geometry, the accuracy of the predictions is not qualified. However, the calculation represents a boundary case that delimits the range of possible responses of a fuel element subjected to a mechanical load. The results illustrate that the hollow fuel element model can be used in a conservative manner to generate larger element deflection to bending loads resulting in higher stress intensity factors at the assembly welds. It is expected that these values will be higher than in reality since the irradiated pellet will stiffen the element, as is observed from the predictions obtained with the pellet interface model.

Table 4: Comparison of Fuel Element Models under Bending Loads

Fuel Element Model	Mid-Element Deformation (mm)	Maximum K_I (MPa $m^{1/2}$)
Hollow Fuel Element	4.10	9.68
Pellet Interface Model	2.48	4.89

6.3 TYPICAL FUEL BUNDLE GEOMETRY STRESS DISTRIBUTIONS

The 2005 Study by Lazaroski *et al.* indicated that the majority of used fuel in the bulk population does not show any indication of atypical deformation or damage that could in itself increase the stress levels at the assembly welds. The assembly weld stress levels in this fuel would originate mainly from residual stresses due to manufacturing, stress present from the post-discharge geometry of the fuel, and induced stress from gravitational forces on the fuel in the module tubes of a DSC. The residual stresses in the assembly welds from manufacturing of CANDU fuel bundles are not known but it can be assumed that the high temperatures experienced by the fuel in the reactor are conducive to relieving these stresses. Consequently, initial stresses arising from the post-discharge geometry of the bundle were evaluated with the stress model using typical normal-burnup and high-burnup profiles.

To determine the stress distributions in the endplate and at the assembly welds resulting from spacer pad interaction, the post-discharge geometries were solved in ANSYS 11.0 under zero external mechanical loads and gravitational acceleration. The solution prevented the overlapping of spacer pads, resulting in bending of elements and generation of stress in the endplates. The solution was performed at a temperature of 130°C. The hollow fuel element model was used for each element in the bundle with identical loading as described in section 6.2, above.

Figure 23 illustrates the axial component of the stress field on the inside surface of the endplate. The axial stress extreme values are seen at the assembly welds. It can be seen that one side of the weld is under compression (negative axial stress) and the opposite side in tension (positive axial stress) which is consistent with the bending of the elements. The maximum axial stress in bundle 28B (typical normal burn-up) is 28 MPa. This value is twice the value of 13 MPa estimated for the high-burnup bundle (28A).

To calculate the stress intensity factors at the assembly weld cracks, the 28-element sub-model was used. The sub-model was run for several assembly welds on each of the two bundles. The element with the maximum tensile stress was examined, along with several outer-ring elements. The results of the sub-model calculations are shown in Table 5. The K_I value in the table corresponds to the value calculated at the weld tip region with the maximum tensile strain. The results suggest that critical stress intensities as large as 1.5 MPa $m^{1/2}$ may be present in used 28-element CANDU fuel due solely to the post-discharge geometry of the bundle, prior to any loading due to storage.

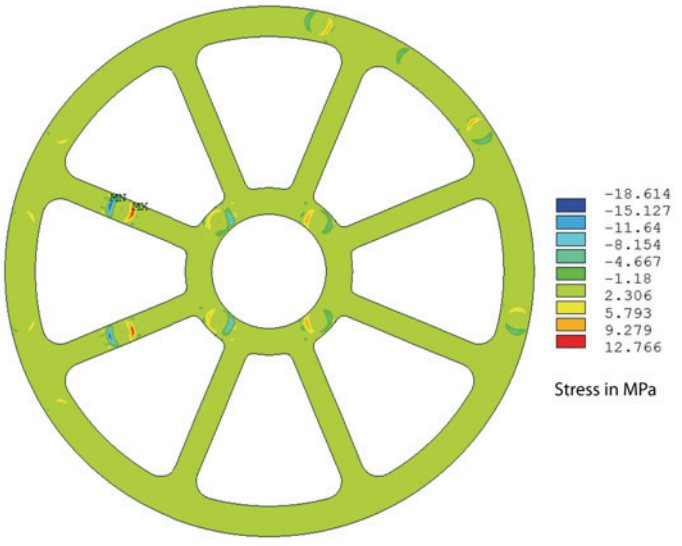

(a) Bundle 28A

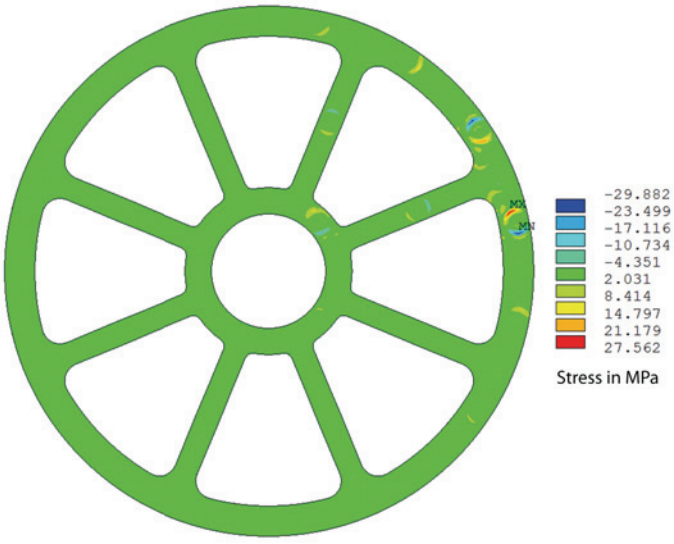

(b) Bundle 28B

Figure 23: Endplate Axial Stress Distribution Due to Post-Discharge Geometry

Table 5: Post-Discharge Assembly Weld Maximum Stress Intensity Factors for a Crack Depth of 0.5 mm

Bundle Element		K_I (MPa $m^{1/2}$)
28A	7	0.40
	9	0.30
	17	0.83
28B	7	1.16
	8	1.48
	20	0.09

6.3.1 Used Fuel Bundle in a Module Tube

The stress distribution resulting from a bundle with no initial element bowing placed horizontally in a module tube was also calculated using the CANDU fuel bundle model. The geometry of the system to model is shown in Figure 24. The numbering used for the fuel elements is also shown. The temperature of the simulation is the approximate initial expected fuel sheath temperature of 130°C. The module tube is not explicitly modelled in ANSYS as this would require additional contact pairs further complicating convergence of the solution. Instead, the contact of bearing pads with the module tube is modelled through the application of constraints on the bearing pad nodes representing module tube contact. Displacements of the fuel bundle in the module tube are illustrated in Figure 25 for a 28-element fuel bundle.

The 28-element sub-model was used to determine the maximum K_I value at the assembly weld cracks of several elements. The results of the sub-model calculations are given in Table 6. The stress intensity factor for element 12 at the bottom of the bundle had the smallest K_I factor of the elements examined. Element 10 had the largest axial tensile stress and the largest K_I value of 1.01 MPa $m^{1/2}$ which also corresponds with a region of largest fuel element displacements. The inner-ring element 18 at the top of the bundle also gave a very similar K_I value.

28-Element Fuel Bundle in a Module Tube

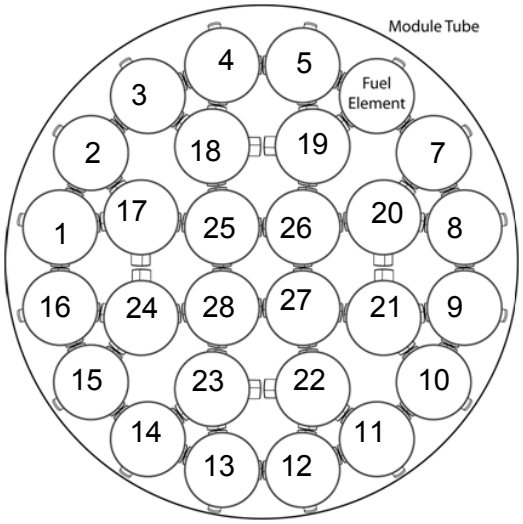

Figure 24: Cross Section of a 28-Element Fuel Bundle in a Module Tube

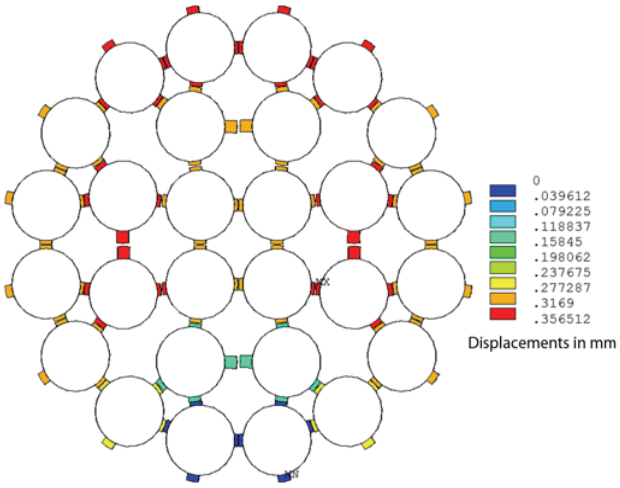

Figure 25: Fuel Element Displacements in the Mid-plane Cross Section of a 28-Element Fuel Bundle in a Module Tube

Table 6: Calculated Assembly Weld Maximum Stress Intensity Factors for a Nominal 28-Element Bundle in a Module Tube

Element	K_I (MPa $m^{1/2}$)
8	0.90
10	1.01
12	0.44
18	0.97

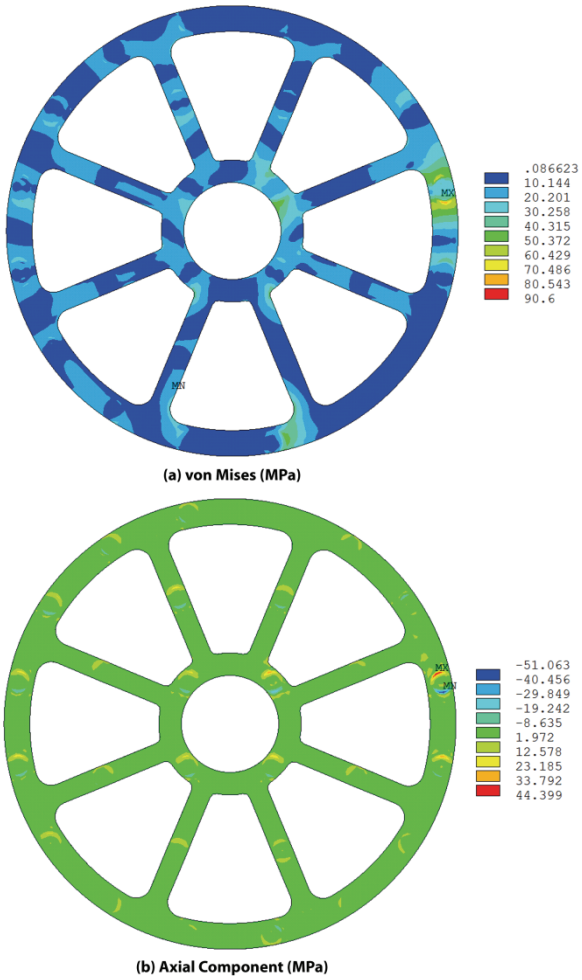

Figure 26(a) and 26(b): Stress Distribution in the Endplate of Nominal 28-Element Average Burnup Fuel Bundle in a Module Tube

The mechanical analysis described above was repeated with a 28-element fuel bundle with typical post-reactor geometry for average-burnup supported in the module tube but including the effect of gravitational acceleration. The temperature of the bundle was as before at 130°C.

The results of the stress fields at the endplate are illustrated in figures 26(a) and (b). Figure 26(a) shows the von Mises stress field on the inner surface of the endplate. The maximum stress is in the vicinity of the assembly weld for element 8. The axial component (Figure 26(b)) shows the maximum axial values for the same weld.

The maximum values of the stress intensity factors at the assembly weld cracks of several elements were evaluated using the 28-element sub-model, and are summarized in Table 7. The highest value for the stress intensity factor is 2.45 MPa $m^{1/2}$ for element 8. For comparison, the stress intensity factor for a fuel element located at the bottom of the bundle, element 12, is 0.80 MPa $m^{1/2}$.

With time, the fuel channels in the nuclear reactors are creeping due to the high operating temperatures and neutron flux. This is resulting in diametral creep of the pressure tube to larger diameters as well as vertical sag of the channel. The effect that the sag of a fuel channel might have on a fuel bundle was also assessed. However, while PIE examinations indicate bundles are slightly bowed as a result of irradiation, for the purpose of this study, it has been conservatively assumed that bundles take on a profile exactly matching a crept fuel channel profile.

The current sag profiles of several channels expected to have the largest amount of creep were reviewed to determine a potential range of bundle bowing. The maximum bundle bow observed was less than 0.8 mm at the point of maximum bow deflection. A fuel bundle with this degree of bowing resting in a module tube was modelled using the fuel bundle model. Similar to the previous simulations, gravitational forces were modelled and the simulation temperature was 130°C.

Table 7: Calculated Assembly Weld Maximum Stress Intensity Factors for an Average-Burnup 28-Element Bundle in a Module Tube

Element	K_I (MPa $m^{1/2}$)
8	2.45
12	0.80

Based on the axial component of the endplate stress field, the sub-model was used to calculate the maximum K_I values at the crack tip in elements 11, 12, and 22. The results are documented in Table 8. A maximum stress intensity factor of 3 MPa $m^{1/2}$ was calculated in element 22. The maximum stress intensity factor for an outer-ring element was 1.5 MPa $m^{1/2}$, which is not different than the maximum K_I calculated from the post-discharge geometry of a 28-element fuel bundle.

Table 8: Calculated Assembly Weld Maximum Stress Intensity Factors for a Crept-Channel Geometry Bundle in a Module Tube

Element	K_I (MPa $m^{1/2}$)
11	1.12
12	1.53
22	3.04

Atypical Fuel Bundle Geometries

In the 2005 Study on the condition of used CANDU fuel bundles (Lazaroski *et al.*, 2005), visual fuel inspection records of discharged fuel bundles were evaluated to estimate the percentage of fuel in the bulk population that may have increased stress levels in the assembly welds. During fuel inspections, the external surface of the bundle is inspected visually and observations are

recorded in accordance with visual standards of deformation, wear, deposits or corrosion, and bundle structural integrity. Records of the observations are made on fuel inspection sheets and evaluated in terms of the effect on the stress levels at the assembly weld. This information was then used to estimate the percentage of fuel potentially more susceptible to dry-storage degradation.

Fuel inspection observations that could potentially increase the stress levels at the assembly welds in used fuel bundles are:

- **Crushed bundles:** where there is evidence, or established records, that unusually high loads were applied to the bundles during fuel handling.
- **Dropped bundles:** where it is known that the fuel bundles were dropped during handling, usually during the process of moving the bundles to the fuel inspection platform.
- **Deformation:** where an observation of abnormal deformation of the bundle was observed. Observations of heavy deformation of the endplate or interlocked spacer pads could potentially increase stress levels, specifically at the assembly welds.
- **Endcap mechanical damage:** where deformation of the endcaps is evident. The interaction causing the damage may affect the residual stress in the assembly weld.
- **Endcap latch marks:** a subset of the previous category where the interaction is due to the fuel channel latches.
- **Missing appendage:** where an element appendage (bearing pad or spacer pad) was not present potentially allowing for greater bowing of the element.
- **Element bowing:** where the abnormal bowing of the element, and possible constraint during dry storage, may increase the stress in the assembly welds.
- **Spacer pad wear:** where significant wear on a spacer pad was observed and would indicate higher-than-normal vibration during irradiation.

For 28-element fuel bundles, no observations of crushed bundles, interlocking spacer pads, endcap latch marks, missing appendages, bowing, or spacer pad wear have been made up to the end of 2004. Several 28-element bundles have been dropped, but these bundles became part of the segregated population and will be stored different than the bulk population.

The main non-typical 28-element fuel conditions potentially affecting assembly weld stresses is due to endplate deformation and endcap mechanical damage. Preliminary calculations assuming small amounts of axial displacement, on the order of tenths of millimetres, applied for a single fuel element can generate significant stresses in the weld crack. To better understand the effect of endplate deformation and endcap mechanical damage may have on assembly weld stress levels due to axial deformation, residual stresses resulting from the interactions causing such damage would need to be evaluated. This evaluation requires a better understanding of the interactions, the resultant damage, and plastic material properties for irradiated Zr-4. The fuel bundle models would be capable of estimating the stress resulting from

such interactions, but further development would be required. However, the expected number of bundles that could be expected to have these characteristics is quite minimal, and, further effort, in this direction is not fully justified.

6.3.2 Summary and Discussion of Findings

The irradiated CANDU fuel bundle model has been used to perform an evaluation of the stress distributions in endplates and resultant stress intensity factors at the assembly weld cracks of fuel bundles in postulated dry storage conditions. A conservative approach to evaluating the mechanical deformation of used CANDU fuel bundles in module tubes was employed due to uncertainties in modelling irradiated fuel bundles.

The irradiated 28-element fuel bundle model has been used to calculate the stress distributions and K_I values for several dry storage scenarios. For all these calculations, the hollow fuel element model that ignores stiffening effects of fuel pellets has been used to give conservative results. An evaluation of the endplate stress for fuel bundles with a post-discharge geometry determined from PIE was performed.

The maximum stress intensity factor at the tip of a 0.5 mm weld crack in the high-burnup bundle was 0.8 MPa $m^{1/2}$. The average-burnup bundle calculations gave a higher maximum crack-tip K_I value of 1.5 MPa $m^{1/2}$. Under gravity and being supported in a module tube, the maximum value of K_I for the average-burnup bundle geometry was approximately 3 MPa $m^{1/2}$. There are several sources of uncertainty in these results. First, the fuel bundle geometry has been idealized to the nominal dimensions defined in the fuel design documents and drawings.

There are tolerances on the values that the manufacturer must adhere to, but manufacturing dimensions will generally differ from the design values. Wear of the Zr-4 material during irradiation can also affect these dimensions. For example, one important dimension is the spacer pad height. Manufacturing dimensions may be different than those modelled, but it is not known if the height is increased or decreased. However, spacer pads do wear during irradiation which will act to increase the gap between mating pads. The amount of wear is highly variable between different bundles as well as within a single bundle and no quantitative data is available on amounts of wear. Therefore, the true gaps between spacer pads are hard to quantify. The radial distance of the element welds from the bundle axis are also variable and can affect the interaction of adjacent elements. Initial endplate deformation may also affect element bending and endplate stress fields. Sensitivity studies using design tolerances could be performed to better understand the effect of bundle dimensions on the endplate stress levels.

Another source of uncertainty in the post-discharge geometry results is the effect of residual stress at the crack tip due to the welding process. Preliminary modelling of the welding process suggests the magnitude of the stress in the weld crack region may be in the vicinity of several hundred MPa. However, stress relaxation due to creep during the residence of the fuel bundle in the reactor is expected to be significant and, therefore, the residual stress has been assumed to be negligible in this analysis.

To understand the magnitude of endplate stress resulting from irradiated fuel bundles stored in a DSC, the interaction of a bundle with the module tube was evaluated. This was considered for three bundle geometries: a nominal straight bundle; a bowed bundle resulting from the sag of the fuel channel in an aged reactor; and a bundle of average-burnup with post-discharge geometry. The nominal bundle suggests stress intensity factors in the outer-ring elements as

large as 1.0 MPa $m^{1/2}$. For the case of a bundle with limiting geometry, the outer-ring elements indicated that the stress intensity factors could be as high as 1.5 MPa $m^{1/2}$, but had a maximum K_I value of 3 MPa $m^{1/2}$ for an intermediate-ring element. For the bundle with the post-irradiation geometry, the highest stress intensity factor was 2.5 MPa $m^{1/2}$ for an outer-ring fuel element. Further calculations on bundles with post-discharge geometries in module tubes are required to fully explore variations in the bundle post-discharge geometry and bundle orientation in the module tube. From the point of view of dry storage, outer-ring elements are the primary concern because a loose outer-ring element may interfere with fuel handling systems. Inner loose elements, however, are unlikely to result in fuel handling concerns because they will be contained by the outer ring elements.

The analyses performed suggest that the stresses generated in the endplates of irradiated 28-element fuel bundles and resultant stress intensity factors are relatively low. The inner regions of the endplate corresponding to the non-outer-ring elements may have lower stress magnitudes, but bending of these elements may possibly lead to greater stress intensity factors. However, further evaluation of the effect on the calculated maximum stress intensity factors from bundle post-discharge geometry variations when simulated in module tubes may be desirable.

6.4 WELD MORPHOLOGY EFFECT ON COMPUTED STRESS INTENSITY FACTORS

Additionally, the effects of fuel element and endplate geometry, weld morphology and endplate-to-endcap weld on computed stress intensity factors were examined. The stress intensity factors were computed from the *J*-integral or *I*-integral using the finite element method. The stress intensity factors for mode I, II and III loading were also determined in order to investigate the deformation of the crack front.

6.4.1 Computed Stress Intensity Factors

Endplate welds present a notch as a weld discontinuity which acts as a stress raiser thus creating the possibility of fracture cracking of the weld depending on loading conditions. In the case of DHC being active, cracking will occur if the threshold stress intensity factor is exceeded. The K_{IH} values are determined experimentally. Additionally, the location and shape of the notch, as well as the shape of the weld whether circular or elliptical will affect the stress fields and consequently the value of the stress intensity factor (K_I). The effects of fuel element and endplate geometry and endplate-to-endcap weld discontinuity on the computed stress intensity factors will be briefly discussed and how they might affect the experimentally found K_{IH} values.

The stress intensity factors were computed using the *J*-integral and plane strain conversion for the majority of analyses performed except when assessing complex deformation of the crack front. Three dimensional models were developed using 20-node elements with reduced integration order.

6.4.2 Endcap-Endplate Weld Discontinuity Stress Intensity Factors

The endplate-to-endcap weld discontinuity is effectively a crack that shows variation in shape. Figure 27 illustrates the actual endplate-to-endcap weld discontinuity from results of testing. In

this analysis, the endcap weld has a round shape. The shape of the endcap-endplate weld discontinuity was modeled to be round or elliptical.

Numerical simulations were performed to determine how these characterizations affect the computed stress intensity factors. The representative depth of the discontinuity and various circumferential extensions were applied. The reference case was a fully circumferential crack with round shape. Appropriate mechanical material properties for the weld were based on Zircaloy-4 material.

Numerical simulations were performed for three cases: a fully circumferential surface crack with constant depth (reference case), a limited extension round surface crack with constant depth and a limited extension surface elliptical crack. In this analysis, the crack depth was chosen as 0.51 mm and is representative of weld discontinuity depths found in the DHC experimental program.

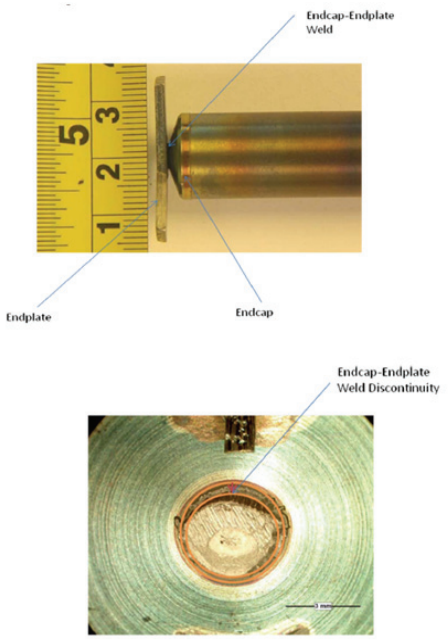

Figure 27: Endplate-to-Endcap Discontinuity

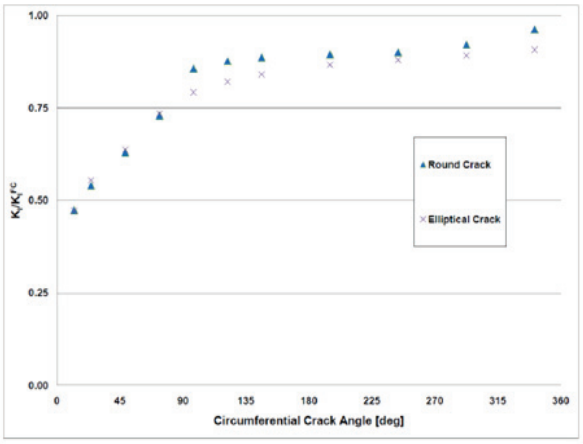

Figure 28: Effect of Surface Crack Extension on Computed Stress Intensity Factor

The stress intensity factors were computed at the location of the maximum crack driving force for a particular crack extension. These cracks have limited crack extension angle. However, the location of the maximum stress intensity factor could change depending on surface crack dimensions. Figure 28 summarizes the results of the simulation by plotting the computed stress intensity factors for constant depth and elliptical cracks normalized by the stress intensity factor of 9.7 MPa $m^{1/2}$ for a fully circumferential crack. A zero degree angle was assigned to a crack tip location in the vertical plane. The results show that constant depth round surface cracks showed slightly higher stress intensity factors over elliptical cracks. This means that the shape of the weld discontinuity introduces some uncertainty to the calculated stress intensity factor; however, it is small but it should be confirmed for the actual fuel element geometry. For crack

tip locations beyond 90 degrees from the application of the load, the effect of limited crack extension is strong. However, in practice this situation is unlikely to occur.

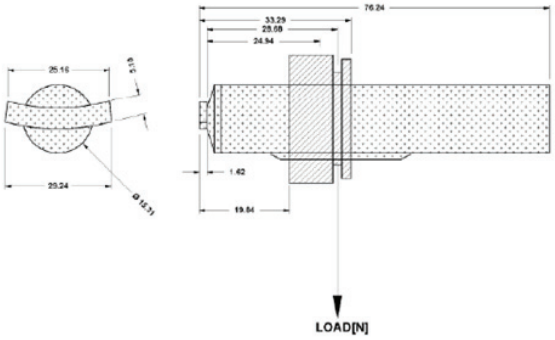

Figure 29a: Set-up loading and GE-28 geometry

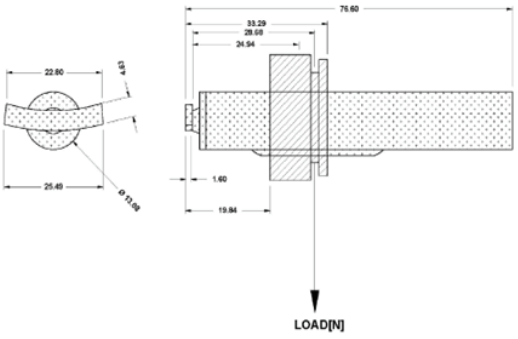

Figure 31a: Set-up loading and GE-37 geometry

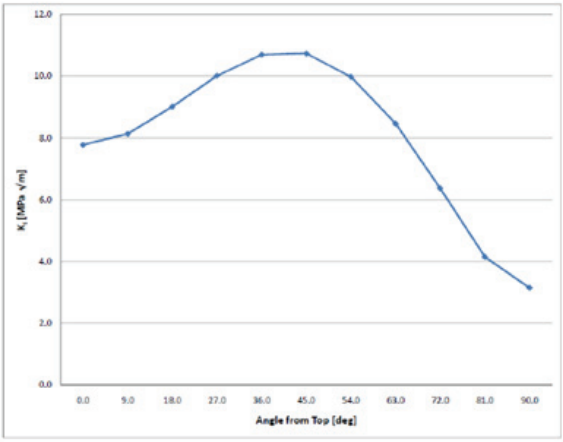

Figure 30b: K_I Distribution for GE-28 geometry

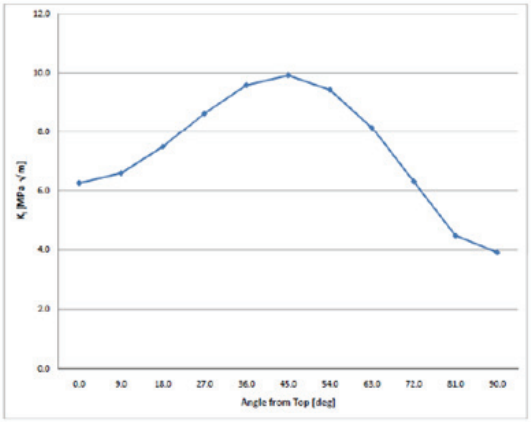

Figure 32b: K_I Distribution for GE-37 geometry

6.4.3 Effect of Bundle Design on Computed Stress Intensity Factors

The effect of bundle design on computed stress intensity factors is best illustrated by reference to the GE-28 and GE-37 element bundles being tested (Figures 29a to 32b). Both bundles differed from each other in their geometries. In particular, for fuel elements of GE-28 design, the position of the endcap-weld is moved from the center of the endplate thus leading to a different loading condition.

In calculating the stress intensity factors for these bundles endplate welds, the crack depth was defined as a combination of the notch depth and the depth of the endcap-to-endplate weld discontinuity. GE-28 element bundle fuel elements are different from GE-37 type. They have both different geometry and endcap-endplate weld discontinuity as can be observed from Figures 29a and 31a. In the GE-28 design, the position of the endcap is moved from the centre

of the endplate. This suggests that there might be some sensitivity of the stress intensity factors on the characterization of the geometry and boundary conditions.

Three dimensional finite element models of the GE-28 type fuel element were created using 20-node hexahedral elements. Rigid boundary conditions were applied to two external surfaces of the endplate to simulate actual tests. In this particular model, the endplate width was the same as the diameter of the endplate-to-endcap weld. The actual geometry from test 09_125 was used in these calculations

Similarly, the fuel element geometry and load setup of the GE-37element fuel bundle is shown in Figure 31a. Numerical calculations were performed for the geometry of the fuel element tested in the test 09_120. Figures 30b and 32b show the distribution of the computed stress intensity factors for the load at DHC initiation during the experiments. The distributions of the K_I values for both bundles are similar with the maximum value observed at 45°. At this angle, the crack showed a complex deformation state mode I, II and III. The effect of location of the endcap weld regarding the endplate was also studied. The results showed K_I values distributions similar to the ones shown above for GE-28 and GE-37 element bundles.

6.5 THRESHOLD STRESS INTENSITY FACTORS FOR DHC AT THE WELDS

6.5.1 Results of DHC Tests

As stated earlier, the intent of the Delayed Hydride Cracking (DHC) Experimental program was to develop a database on threshold stress intensity factors (K_{IH}) for DHC initiation and Delayed Hydride Cracking Velocities (DHCV) by testing the endplate welds of different bundle designs and manufacturers at temperatures relevant to the dry storage of the fuel in DSCs. The database includes results from three GE 37-element bundles, one GE 28-element bundle and one CAMECO 37-element bundle. These bundles were manufactured without pellets but conform to all the manufacturing details and quality control of full bundles.

Two of the three 37-element General Electric (GE) unirradiated fuel bundles were tested as part of the development of a test apparatus and test procedure in 2008 (Shek et al., 2008, and, Shek and Wasiluk, 2009). The remainder tests covering both GE and CAMECO fuel bundles were completed in 2009 (Shek et al., 2010, and, Shek, 2011).

In the 2008 tests, a total of five endplate welds were tested. One at 130°C with a 10 ppm hydrogen concentration and four welds at 150°C and 40 ppm hydrogen concentration. The K_{IH} value for the 130°C was 8.3 MPa$\sqrt{m}$ and the K_{IH} values of the four other welds ranged from 7.6 to 13.6 MPa$\sqrt{m}$. Crack velocities were of the order of 10^{-9} m/s. Further details of the data are included in Table 10.

When examining the welds from the two manufactures and bundle types by visual inspection and metallography, differences in weld size, notch depth and profile, and weld discontinuity were observed among the three types of fuel bundles. There are also differences in notch depth between the OD and ID side of the endplate weld. This will likely affect the applied load for DHC initiation as the stress concentration will be affected by the dimension of the notch and the depth of the weld discontinuity. However, this should not affect the K_{IH} value which is a material property.

A complete K_{IH} test consists of three parts: (i) test the specimen by steadily incrementing the applied load until DHC crack initiation is observed, at which point, the load is maintained to observed steady crack; (ii) post test examination of the DHC fracture surface and measure dimensions of endplate welds to determine the notch and initial crack depths and weld area; (iii) determine the K_{IH} value by finite-element analysis using the crack initiation load and endplate weld dimensions. A description of the finite-element methodology on the calculation of stress intensity factor for DHC initiation from the endplate welds can be found in Shek and Wasiluk, 2009. A summary of the results from all three bundles is provided in Table 9.

The following observations and conclusions can be made from the tests performed on the GE 37-element, GE 28-element and CAMECO 37-element bundles in 2009 and the tests performed on the GE 37-element bundles in 2008:

(1) There was variability in weld geometry such as the profile of the notch formed between the endplate and endcap, the weld discontinuity and weld area among the GE 37-element, GE 28-element and the CAMECO 37-element fuel bundles. In terms of the weld geometry, the endplate welds of the CAMECO 37-element bundle appear to be the least susceptible to DHC as the notch root radius was blunter and the weld discontinuity was either non-existent or small. There was also a difference in the location of the welds with respect to the width of the endplate. The welds of the GE 28-element and CAMECO 37-element bundles were more skewed towards the OD side of the endplate than the welds of the GE 37-element bundle.

(2) The DHC cracks did not necessarily initiate at the top of the welds with respect to the loading orientation. The DHC cracks of the GE 37-element bundle and the CAMECO fuel bundles appear to have initiated at the location about 45° deviated from the top of the weld. However, most of the cracks of the GE 28-element bundle were initiated from the top of the weld, similar to that observed in the GE 37-element bundle tested in 2008 (Shek and Wasiluk, 2009, and, Shek et al., 2008).

(3) Among the three bundles tested in the current program, the applied bending stresses for DHC initiation from the endplate welds were highest for the GE 37-element bundle, followed by the CAMECO 37-element bundle and then the GE 28-element bundle. However, the bending stresses for DHC initiation from these three bundles were higher than that of the GE 37-element bundle tested in 2008. The limited data indicated that the applied bending stress for DHC initiation was higher when the weld was loaded on the OD side of the endplate than loaded from the ID side.

(4) The K_{IH} values of the endplate welds of the three fuel bundles tested in 2009 were similar and appear to be higher than that of the GE 37-element bundle tested in 2008. Based on the limited data, there was no significant difference in K_{IH} values whether the weld was loaded from the ID side or OD side of the endplate.

(5) There was no large difference in DHCV at 150°C among the welds of the three bundles tested in 2009. The DHCVs appear to be lower that of the GE 37-element bundle tested in 2008.

6.6 INTEGRATION OF THE BUNDLE STRESS MODEL WITH EXPERIMENTAL DATA

Comparison of the modelled K_I values for 28-element bundles (sections 6.3 and 6.4) with the experimental K_{IH} values (section 6.5) provides a means to evaluate the potential for the presence of operative DHC in CANDU used fuel. The assessment focused primarily on the Pickering 28-element fuel bundles. The assessment strongly suggests that DHC is not expected to occur in 28-element fuel bundles, and, by extension of the results, to the 37-element fuel bundles as well. However, some uncertainties remain that were not fully explored in the studies.

Full-bundle mechanical stress modelling of 28-element CANDU fuel models for varying conditions in horizontal dry storage was summarized in Section 6.4. Stress distributions were computed throughout the bundle and for assembly welds with the largest stresses, the maximum stress intensity factor at the tip of a 0.5 mm weld discontinuity was calculated. For the purposes of dry storage, DHC of an outer-ring weld is of key importance, as it could result in a loose element that affects handling of the fuel bundle. It may be possible that a cracked weld on the interior of the bundle affects the bundle's response to impacts and vibration, but it is unlikely it would affect handling of the bundle structure.

One scenario evaluated a nominal bundle geometry (*i.e.*, no initial deformation and perfectly straight elements) in a DSC module tube. In this scenario, the maximum K_I value was calculated to be 1.01 MPa $m^{1/2}$ in an outer-ring element. The maximum tensile axial component of the stress field across the weld was found to be approximately 20 MPa and the element mid-plane displacement was approximately 0.3 mm.

The nominal bundle geometry is not considered a realistic scenario for the majority of used CANDU fuel bundles because post-irradiation examinations show that the bundles creep during irradiation. Using post-irradiation examination information as inputs into the fuel bundle geometry, another scenario was evaluated where a fuel bundle with a post-irradiation geometry was modelled in a DSC module tube (section 6.3.1). In this scenario, the maximum K_I value calculated was 2.45 MPa $m^{1/2}$ for an outer-ring element. The maximum tensile axial stress component across the weld was 44 MPa and the element mid-plane displacement was approximately 0.9 mm.

One other scenario was investigated where a bundle with an identical amount of bow of each element was modelled inside a DSC module tube. The amount of bow was taken from current sag profiles of CANDU fuel channels. This scenario was to represent a situation where a bundle from an aged, bowed pressure tube is placed in a straight module tube. The geometry of the bundle is not truly representative of the bundle geometry from an aged channel as it does not consider diametrical expansion of the pressure tube and its effect on the bundle geometry. However, it was investigated to see if ageing of the reactors could affect DHC initiation in used fuel. The calculations indicated the maximum K_I value would be for an intermediate-ring element with a value of 3.04 MPa $m^{1/2}$. However, the maximum K_I for an outer-ring element was 1.53 MPa $m^{1/2}$ with a maximum axial stress component approximately 28 MPa and a middle element displacement of approximately 0.6 mm.

The K_I calculations performed suggest the outer-ring values in used fuel may be as large as 2.5 MPa $m^{1/2}$. As well, the effects of post-discharge geometry on stress intensities at the assembly welds may also be larger than stresses induced by constraint of the bundles in module tubes under gravitational loading.

Table 9: Summary of the 2009 DHC Tests on Endplate/Endcap Welds (Shek et al., 2010, and, Shek, 2011)

Test #	Bundle type	Element #	DHC rig	Tensile stress on ID or OD side	DHC initiation load (N)	Bending stress for DHC initiation (MPa)	K_{IH} MPa√m	DHCV at 150°C prior to heat tinting (m/sec)	DHCV at 150°C after heat tinting (m/sec	Postulated location for DHC initiation based on fracture surface examination
09-106	GE 37-element	2	4	ID	64	282	11.2	6.12 E-10	1.33 E-9	~45° from top
09-120	GE 37-element	5	6	ID	63	282	10.7	4.46 E-10	1.54 E-9	~45° from top
09-136	GE 37-element	8	4	ID	72	334	11.1	5.01 E-10	1.56 E-9	~45° from top
09-148	GE 37-element	15	4	ID	76	367	13.1	8.57 E-10	2.93 E-9	~45° from top
09-124	GE 37-element	17	4	OD	83	346	12.2	1.23 E-9	2.31 E-9	~45° from top
09-125	GE 28-element	2	6	ID	53	227	10.1	1.29 E-9	NA	Top of weld
09-130	GE 28-element	4	6	ID	53	214	10.0	1.45 E-9	2.55 E-9	Top of weld
09-144	GE 28-element	15	6	ID	56	220	13.6	1.41E-9	3.26 E-9	Top of weld
09-172	GE 28-element	6	6	ID	53	225	9.4	1.20 E-9	5.05 E-9	Top of weld
09-182	GE 28-element	8	6	OD	67	285	11.6	4.46 E-10	2.17 E-9	~45° from top
09-135	CAMECO	6	6	ID	73*	253	NA	NA	NA	~45° from top
09-186	CAMECO	18	4	ID	85	277	12.2	NA	NA	~45° from top
09-204	CAMECO	5	4	ID	80	255	12.1	8.41 E-10	1.78 E-9	~45° from top
09-208	CAMECO	16	6	ID	80	325	NA	7.0 E-10	NA	~45° from top
10-16	CAMECO	9	4	ID	93*	324	13.5	NA	NA	~45° from top

*based on estimated cracking time; NA: Not Available

Table 10: Summary of the 2008 Tests on Endplate/ Endcap Welds (Shek et al., 2008, and, Shek and Wasiluk, 2009)

Test ID	Bundle type	Type of Test	H concen-tration (ppm)	Test Temp. (°C)	Maximum nominal bending stress at crack initiation (MPa)	K_I for DHCV test or K_{IH} (MPa$\sqrt{m}$)	DHCV (m/sec)		Postulated location for DHC initiation based on fracture surface examination
							Before heat-tinting	After heat-ting	
07_09	GE-37	K_{IH} test	10	130	184	8.3	4.7E-10	5.4E-10	Top of weld
07_67	GE-37	K_{IH} test	40	150	163	7.7	2.5E-10	NA	Top of weld
07_104	GE-37	K_{IH} test	40	150	167	7.9	6.8E-10	2.3E-09	Top of weld
07_140	GE-37	K_{IH} test	40	150	170	7.6	2.1E-10	4.0E-10	Uncertain
07_164	GE-37	K_{IH} test	40	150	155	13.6	6.6E-10	2.1E-9	Top of weld
07_78	GE-37	DHCV	40	150	214	11.8	2.1E-9	4.0E-9	Top of weld
07_79	GE-37	DHCV	40	150	209	12.2	1.8E-9	5.5E-9	Top of weld

6.7 LONG-TERM PROJECTIONS OF CANDU FUEL INTEGRITY

6.7.1 Effect of Zircaloy-4 Material Property Variations

The stress model developed for this work assumed there was no variation in the material properties of the Zircaloy-4 throughout the bundle (Popescu and Lampman, 2010). This is known not to be true of manufactured CANDU fuel bundles: the fuel sheath is specially textured compared to the rest of the Zircaloy-4 material which results in different mechanical properties, and, there are multiple heat affected zones—assembly welds, closure welds, and appendage brazing areas—that would also affect the material properties. However, the unirradiated model validation exercises showed excellent agreement between the modelled predictions of element bending and the experimental measurements (Popescu and Lampman, 2010, and, Freire-Canosa, et al., 2010). This suggests that modelling the variations in Zircaloy-4 material properties throughout the bundle is not required to predict the bundle's response to element bending loads.

On a more local level, material property variations throughout the assembly weld would be expected to have an observable effect on DHC initiation. The DHC testing summarized in this report calculated K_{IH} values from measured applied loads on the test samples. A finite element model of the sample was prepared which accounted for an idealized geometry of the sample (*i.e.*, a smooth, circular crack front), but it did not model the material variations in the weld as the material properties are unknown. Similarly, the assembly weld sub-models used to calculate K_I values accounted for an idealized weld geometry and homogeneous material properties. As such, the K_I and K_{IH} values determined may not be true values for the CANDU assembly welds, but they were determined using the same assumptions and can be used for comparative assessment.

6.7.2 Effect of Fuel Pellets on Fuel Element Bending

The fuel pellets within the fuel sheath have a large effect on the stiffness of an element. The fuel element model contained individual pellets and their contacts with adjacent pellets and the surrounding sheath. This was required to match the mechanical response of the unirradiated fuel element during validation tests. Prior to irradiation, the fuel pellets are solid, homogeneous, and, have a well defined geometry. However, after irradiation, the pellets contain many cracks and chips and the grain structure is no longer homogenous in the pellet. Insufficient data exists on mechanical behaviour of irradiated fuel pellets to accurately model their behaviour. Due to the uncertainties in modelling irradiated pellets, they were removed from the irradiated fuel models used to evaluate stresses and K_I values in dry-stored CANDU fuel bundles.

To investigate the effect irradiated pellets may have on the fuel element bending and assembly weld K_I values, a comparison of bending of a fuel element without pellets and one with solid pellets in very near contact with the sheath was performed (Lampman and Popescu, 2010). Under identical loading conditions, the introduction of the pellets reduced the mid-element displacement, or bending, by approximately 40% and the maximum assembly weld K_I reduced by approximately 50%. The solid pellet in contact with the sheath is probably a bounding case, but this suggests that the presence of irradiated fuel pellets would reduce the K_I values at the assembly welds, possible by a factor of two. Therefore, the modelled response of used CANDU fuel bundles in dry storage is expected to be conservative with respect to DHC.

6.7.3 Effect of Weld Morphology and Crack Depth

The DHC testing performed by Kinectrics (Shek, 2010) provided a large amount of good information on the assembly weld morphology. The variability in the morphology was clear from the post-test weld cross sections. In some cases, the weld and discontinuity seemed to have an elliptical shape in the plane of the weld, whereas in other cases the shape was more round.

Kinectrics investigated the effect of elliptical versus round weld profiles on the computed K_I values and found difference to be within approximately 10% of each other (Wasiluk, 2010). Therefore, there is an uncertainty in stress intensity factors calculated using idealized geometries compared to the real geometries, but the effect appears to be minor.

A feature of the assembly welds that would have a more significant effect on the calculated stress intensity factors is the discontinuity depth. The stress model calculations assumed a depth of 0.5 mm. However, the discontinuity depths appear to be mainly in the range of 0.2 mm to 0.3 mm (Shek, 2010). The relationship between stress intensity factor and crack depth for a circumferential crack in a rod is,

$$K_I \propto \sqrt{c}$$

where *c* is the crack depth. Therefore, accounting for a more realistic weld discontinuity depth, the K_I values would be reduced by approximately 25% to 35%.

6.7.4 28-Element Bundle DHC Initiation Test Measurements

As given in Tables 9 and 10, the unirradiated DHC testing of 28-element CANDU fuel found K_{IH} values in the range of 7.6 MPa $m^{1/2}$ to 13.6 MPa $m^{1/2}$ for DHC initiation in outer-ring elements (Shek, 2010). Based on the tests performed, it is not possible to determine if there is a difference in initiation between the inner and outer diameter of the endplate. These values are consistent with the K_{IH} values ranging between 10.7 MPa $m^{1/2}$ to 13.1 MPa $m^{1/2}$ for the tested 37-element fuel samples (Shek, 2010). Therefore, it appears there is no systematic difference in the K_{IH} value between the different fuel designs and manufacturers.

While the K_{IH} values appear to be consistent between manufacturer and fuel design, there are observable differences in initiation load and bending stress. For the 28-element bundle, the initiation load and bending stress for the inner diameter side of the endplate was approximately 53 N and 220 MPa, respectively. However, for the outer diameter side of the endplate, the equivalent values were slightly higher at 67 N and 285 MPa and the crack initiated 45 degrees from the radial direction, which is likely a result of the different loading conditions. This observation suggests greater bending of the element is required to initiate DHC for elements bowed into the bundle than away. An increased load to initiation of DHC on the outer diameter of the 37-element bundle was also observed, and differences in initiation loads between the 37-element bundle manufacturers are apparent. Based on these observations, the use of K_{IH} is the best measure to evaluate the initiation of DHC for loading conditions that have not been directly tested.

6.7.5 Effect of Irradiation

The K_{IH} values determined from this work are for unirradiated material, and a question remains as to the effect irradiation will have on the critical stress intensity factor. There does not appear to be any published data on irradiated Zircaloy-4 K_{IH} values. However, some information on irradiated Zircaloy-2 cladding and electron-beam welded material is available and is presented in Table 11. Zircaloy-4 is a very similar alloy to Zircaloy-2 with the same crystal structure, a slightly higher iron content (approximately 0.04 to 0.11 %wt), and the removal of Nickel (accounting for approximately 0.08 %wt of Zircaloy-2) to reduce the amount of hydrogen uptake (Wah Chang, 2003).

Table 11: Summary: DHC Critical Stress Intensity Factors for Irradiated Zircaloy-2

Material	Temperature (°C)	Irradiation	Hydrogen (ppm)	K_{IH} (MPa m1/2)
Zircaloy-2 Cladding *(Efsing and Pettersson, 2000)*	200	33.9 MWd/kgU	560–1,000	12.5 ± 0.2
		35.9 MWd/kgU	1,200–1,900	12.7
	300	33.9 MWd/kgU	560–1,000	9.9 ± 0.3
		35.9 MWd/kgU	1,200–1,900	9.9 ± 0.2
Electron Beam Welded Zircaloy-2 *(Schofield et al., 2002)*	200–255	3–5 x 10^{25} m^{-2}	55	8–12

The work on high-hydrogen, high-irradiation Zircaloy-2 cladding (Efsing and Pettersson, 2000) found K_{IH} values similar to the unirradiated Zircaloy-4 weld results. Efsing and Pettersson commented that the effect of irradiation in Zircaloy material was observed to be less than theoretical models. For the 200°C temperature tests, the effect of irradiation lowered the measured K_{IH} by approximately 10% of the unirradiated value with the effect increasing at higher temperatures. The work on high-irradiation electron beam welded Zircaloy-2 (Schofield *et al.*, 2002) measured K_{IH} values within a range very similar to those measured as part of this work.

DHC initiation is sensitive to the material and micro-structure, and the K_{IH} values determined for Zircaloy-2 are not directly applicable to Zircaloy-4. However, given the alloys are very similar, and, the apparent similarity in K_{IH} values in the literature and determined by Kinectrics (Shek, 2010), it is expected that the effect of irradiation will be similar on K_{IH} between the two alloys. Therefore, irradiation will slightly lower the measured unirradiated assembly weld K_{IH} values, possibly by an approximate amount of 1-2 MPa $m^{1/2}$.

6.7.6 Evaluation of the Presence of DHC during Dry Storage

The results of the CANDU fuel bundle stress model analysis on 28-element fuel bundles suggest stress intensity factors in the assembly welds would not exceed 3 MPa $m^{1/2}$. Based on the conservatism in the models from lack of fuel pellets and deeper cracks than measured, the upper bound may be more realistically around 1 MPa $m^{1/2}$. The K_{IH} testing suggested stress intensity factors between 9 MPa $m^{1/2}$ to 14 MPa $m^{1/2}$ would be required to initiate DHC.

Considering the effect of irradiation, the K_{IH} values would be lower, probably by several MPa $m^{1/2}$ based on Zircaloy-2 testing. The difference between the K_I and K_{IH} values is significant and DHC is not expected during dry storage of used 28-element CANDU fuel bundles in a DSC. This conclusion makes sense from the perspective of total bending of the fuel element. Large deflections of the fuel elements were noted during the DHC testing. A 2.5 mm deflection of the free end of a 37-element fuel element resulted from the 48 N loading case (Shek, 2010). All tested samples required larger loads, and thus larger deflections, to initiate DHC. Therefore, a fuel element would need to bend by several millimetres to initiate DHC. This level of bending is not expected, or may not even be possible in constrained module tubes.

The stress intensity factors in used 37-element fuel bundles were not evaluated in this work. However, the conclusion that DHC is not present is expected to hold as the K_{IH} values appear to be the same, the weight and overall dimensions of the bundle are similar, and the weld stress intensity factors are unlikely to be several multiples greater than the 28-element values.

6.7.7 Remaining Uncertainties

A key uncertainty remaining from this work is the effect of residual stresses in the assembly weld region due to manufacturing processes. It was noted from the DHC testing program (Shek, 2010) that once the intact bundle was cut, the elements sprung out from the bundle's axis. This suggests that there may be a significant residual stress induced in the bundle from manufacturing. However, the magnitude of the residual stress and its effect on DHC at the assembly welds is uncertain.

It is expected that the magnitude of the residual stress field will be reduced during irradiation. During irradiation, the fuel is exposed to a high neutron flux at nearly 300°C for approximately one year before discharge. During this period, the bundles creep into a new shape determined by the pressure tube constraints. This has been observed in post-irradiation examinations of used CANDU fuel. The residual stress in the bundle from manufacturing is expected to relax during the creep process. However, the amount of creep relaxation was not analyzed in this work and remains unknown.

Another uncertainty in this analysis is the effect of varying used fuel geometries. A relatively minor amount of PIE exists and it was used to evaluate the effect of permanent element bowing on DHC, but other bundle conditions—such as mechanical damage due to interaction with fuel channel or fuel handling objects—have not been accounted for. Much more detailed Zircaloy-4 material properties would be needed, such as non-linear properties, to account for this, but this data does not exist for irradiated Zircaloy-4. These observations on used fuel are rare, but such a condition could promote DHC.

While the bowing of used CANDU fuel elements has been considered in the models, the deformation of endplates has not. Currently, the modelled endplates are perfectly flat, but during manufacturing the endplate at the welds tends to be pushed into the bundle relative to the non-weld endplate sections. Furthermore, irradiation can lead to endplate dome formation (concave or convex distortion) or parallelogram distortion (axial skewing) of the endplates. The effects of this geometry on DHC initiation during dry storage has not been analyzed.

The effect of irradiation on the Zircaloy-4 material properties is also a source of uncertainty. An expected effect on the K_{IH} value for the weld material has been discussed based on a literature review of similar materials, but direct observation of this effect was not made. The effect of

irradiation on material properties used in stress modelling was taken from MATPRO (MATPRO, 2003), which should be reasonable, but verification of the properties was not possible. The effect on the UO_2 fuel pellets is unknown, but a conservative approach was taken to bound the stress analysis so the irradiation uncertainties are relatively minor.

7. CONCLUSIONS

The NWMO's Used Fuel Integrity Program has evaluated the condition of used CANDU fuel bundles during dry storage. More specifically, this work examined whether Delayed Hydride Cracking (DHC) is a likely degradation mechanism during dry storage in Dry Storage Containers for periods extending up to 100 years. The results of the experimental DHC study and finite element stress modelling of CANDU fuel bundles suggest that DHC will not occur.

The work performed on DHC initiation has focussed on the condition of used fuel at the start of dry storage where the temperature of the fuel is between 130°C to 150°C. The post-discharge geometry of the fuel elements have been considered and stresses throughout the bundle calculated for 28-element CANDU fuel bundles resting horizontally in dry storage containers. The calculated stresses and deformations are relatively low with no mid-element bending more than 1 mm. The assembly welds of the fuel bundles are known to have weld discontinuities, which are effectively cracks due to the sharpness of the discontinuity tip, and the stress intensity factors at the crack tips resulting from element bending were calculated. All calculated values were relatively low and remained below 3 MPa $m^{1/2.}$ These calculations were based on conservative models without the stiffening effect of the UO_2 fuel pellets and deeper crack depths than observed in this program

To evaluate whether the calculated stress intensity factors were sufficient to initiate DHC, an experimental program was created to determine critical stress intensity factors for DHC in CANDU fuel assembly welds. This work suggests that the K_{IH} value for the Zircaloy-4 assembly weld is insensitive to manufacturer and the value for unirradiated welds is between 7.6 MPa $m^{1/2}$ and 13.6 MPa $m^{1/2}$. The effect of irradiation on K_{IH} was not evaluated, but based on similar materials it is expected to lower K_{IH} by a relatively minor amount, likely only several MPa $m^{1/2}$. The CANDU 6 fuel bundles manufactured by Cameco Fuel Manufacturing did not appear to contain a weld discontinuity, suggesting they are much less sensitive to DHC.

There are several remaining uncertainties in this analysis. The effect of residual stresses from the manufacturing process has not been evaluated. While unknown, it is not expected to have a significant effect on initiation due to creep relaxation of the fuel bundles while in the reactor cores. The affect of used-fuel mechanical interactions with other objects on the stress intensity factors is also unknown. However, the percentage of the bulk population of used fuel with such interactions is less than 1% (Lazaroski *et al.*, 2005), and this percentage considers minor interactions that are unlikely to promote DHC. Therefore, the presence of DHC is only uncertain in a very minor percentage of fuel.

The findings of the UFI Program suggest that used CANDU fuel bundles in dry storage will have a maximum stress intensity factor of about 3 MPa $m^{1/2}$ whereas a minimum stress intensity factors of 7.6 MPa $m^{1/2}$, which may be lowered by about 2 MPa $m^{1/2}$ is required to initiate DHC. Therefore, DHC is not projected to occur and used CANDU fuel bundles are expected to retain their integrity during dry storage.

ACKNOWLEDGEMENTS

In completing this report, the author has made extensive use of excerpts from the work of the main technical contributors to the NWMO Used Fuel Integrity Program. In particular, the author is indebted to the contributions, support and constructive discussions of Timothy Lampman, Adrian Popescu and Paul Gillespie from AMEC-NSS on the development, testing and validation of the CANDU Fuel Bundle Stress models, and, on the Delayed Hydride Cracking experimental work and the endplate/endcap welds fracture modelling by Gordon Shek, Bogdan Wasiluk and Harry Seahra of Kinectrics Inc.

REFERENCES

Benthem, J.P. and W.T. Koiter. 1972. Asymptotic Approximations to Crack Problems, Methods of Analysis of Crack Problems. Edited by Sih, G.C., Noordhoff International Publishing.

Byrne, T.P. and J. Freire-Canosa. 1984, Effects of Hydrogen/Deuterium Migration, Fast Fracture, Stress Rupture and Oxidation on the Stability of Irradiated CANDU Fuel Stored in a Dry Air Environment. Ontario Hydro Research Division, Rep. No.84-188-K.

Cann, C.D. and J.C. Tait. 2002, Models for the Creep Rupture Failure of CANDU Fuel Cladding during Dry Storage, Ontario Power Generation, Report No. 06819-REP-03723-10003 R00, November.

Efsing, P. and K. Pettersson. 2000. Delayed Hydride Cracking in Irradiated Zircaloy Cladding. Zirconium in the Nuclear Industry: Thirteenth International Symposium, ASTM STP 1423. West Conshohocken, United States of America

Erdogan, F. 1982. Theoretical and Experimental Study of Fracture in Pipelines Containing Circumferential Flaws. U.S. Department of Transportation, DOT-RSPA-DMA, 50/83/3.

Freire-Canosa, J., A. Popescu and T. Lampman. 2010. Deformation of Unirradiated CANDU Fuel Elements under Bending Loads. 11th International Conference on CANDU Fuel. Niagara Falls. Canada. Oct. 17-20.

Garamszeghy, M. 2010. Nuclear Fuel Waste Management Projections in Canada – 2010 Update. Nuclear Waste Management Organization. NWMO TR-2010-17. Toronto. Canada.

Hunt, C.E.L., J.C. Wood, B.A. Surette. and J.Freire-Canosa. 1981, Seventeen Years of Experience with Storage of Irradiated CANDU Fuel under Water. The International Corrosion Forum. National Association of Corrosion Engineers (NACE). Toronto, Canada. April 6-10.

Ikeda, B.M. 2002. Corrosion of Cladding in a Dry Storage Environment. Ontario Power Generation, Nuclear Waste Management Division Report 06819-REP-03723-10001-R00. Toronto, Ontario

Lampman, T., A. Popescu and J. Freire-Canosa. 2008. Development of a CANDU Fuel Bundle Finite Element Model to Assess Post-Irradiation Mechanical Stress Distributions. 24th Symposium on Effects of Radiation on Nuclear Materials and the Nuclear Fuel Cycle. ASTM International. Denver, Colorado, USA. June 24-26.

Lampman, T. and A. Popescu, 2010. A. Initial Evaluation of Mechanical Stress Distributions in Spent CANDU Fuel Bundles. Nuclear Waste Management Organization. NWMO TR-2010-11.

Lampman, T.J. and T.A. Daniels. 2005. Proposed tests and examinations to provide assurance of fuel integrity during dry storage and subsequent handling. Ontario Power Generation, Nuclear Waste Management Division Report 06819-REP-03720-00009-R00. Toronto, Canada.

Lampman, T.J. and A. Popescu. 2008. CANDU Fuel Bundle Stress Model for Used Fuel Dry Storage Analysis. AMEC NSS Document NW007/RP/001 R00. Toronto, Canada.

Lampman, T. and A. Popescu. 2010. Initial Evaluation of Mechanical Stress Distributions in Spent CANDU Fuel Bundles. Nuclear Waste Management Organization Report TR-2010-11. Toronto, Canada.

Lampman, T. J., A. Popescu, and J. Freire-Canosa. 2009. Comparison of CANDU Fuel Bundles Finite Element Model with Unirradiated Mechanical Load Experiments. Journal of ASTM International, Volume 6, Number 3. West Conshochoken, USA.

Lazaroski, M., T. Lampman, S. Wadsworth. and E. Kohn. 2005. Reference Fuel Characteristics at the Start of Dry Storage. Ontario Power Generation Inc., Nuclear Waste Management Division report 06819-REP-03720-00007-R00. Toronto. Ontario. Canada.

Lovasic, Z. and J.E. Villagran. 2004. Used Fuel Integrity during Dry Storage: Investigation Program. Ontario Power Generation Inc. Nuclear Waste Management Division. Technical Memo 06819-REP-03720-00006-R00. Toronto. Canada

MATPRO. SCADAP/RELAP-3D Code Manual Volume 4: MATPRO – a library of Material Properties for Light-Water-Reactor Accident Analysis. INEEL/EXT-02-00589, Volume 4, Revision 2.2. 2003.

McMinn, A., E.C. Darby and J.S. Schofield. 2000. The Terminal Solid Solubility of Hydrogen in Zirconium Alloys. Zirconium in the Nuclear Industry: Twelfth International Symposium, ASTM STP 1354. West Conshohocken, United States of America.

Peehs, M. and C. Rudolf. 1991. "LWR Spent Fuel Management in the Federal Republic of Germany". Paper presented at IAEA BEFAST-II meeting, Vienna, Austria (March 18-22).

Popescu, A. and T. Lampman. 2010. CANDU Fuel Element Model Development and Sensitivity Study. Nuclear Waste Management Organization. NWMO TR-2010-12. Toronto, Canada.

Rashid, Y.R., D.J. Sunderland. and R. Montgomery. 2000. Creep as the Limiting Mechanism for Spent Fuel Dry Storage. Electrical Power Research Institute Report 1001207. Palo Alto, United Stated of America.

Schofield, J.S., E.C. Darby. and C.F. Gee. 2002. Temperature and Hydrogen Concentration Limits for Delayed Hydride Cracking in Irradiated Zircaloy. Zirconium in the Nuclear Industry: Thirteenth International Symposium, ASTM STP 1423. West Conshohocken, United States of America.

Shek, G.K., B.S. Wasiluk, T. Lampman and J. Freire-Canosa. 2008. Testing the Susceptibility of CANDU Fuel Bundle Endcap/Endplate Welds to Delayed Hydride Cracking. 10th International Conference on CANDU Fuel. Ottawa, Canada. Oct. 5-8.

Shek, G.K. and B.S. Wasiluk. 2009. Development of Delayed Hydride Cracking Test Apparatus and Commissioning Tests for CANDU Fuel Bundle Assembly Welds. Nuclear Waste Management Organization. NWMO TR-2009-08.

Shek, G.K., B.S. Wasiluk, J. Freire-Canosa and T. Lampman. 2010. Delayed Hydride Cracking Properties of the Endplate Resistance Welds of CANDU Fuel Bundles. 11th International Conference on CANDU Fuel. Niagara Falls, Canada. Oct. 17-20.

Shek, G.K. 2010. Determination of the Threshold Stress Intensity Factor and Velocity of Delayed Hydride Cracking of Endplate Welds in CANDU Fuel Bundles with Different Design and Manufacturers. Nuclear Waste Management Organization. NWMO TR-2010-25. Toronto, Canada.

Snell, J. 2007. Mechanical Deformation Tests on 37 and 28 Element Fuel. Stern Laboratories. Report SL-190. Hamilton, Canada.

Snell, J. 2009. Mechanical Deformation Tests on 37 and 28 Element Fuel Elements. Stern Laboratories. Report SL-205. Hamilton, Ontario, Canada. 2009.

Tada, H., P.C. Paris, P.C. and G.R. Irwin. 1985. The Stress Analysis of Cracks Handbook, 2nded., Paris Productions Incorporated (and Del Research Corporation). St. Louis, MO.

Wah Change. 2003. Technical Data Sheet: Reactor Grade Zirconium Alloys for Nuclear Waste Disposal. Available at www.alleghenytechnologies.com/wahchang.

Wasiluk, B.S. 2010. The Effect of CANDU Fuel Bundles Endplate/Endcap Weld Morphology on Computed Stress Intensity Factors at the Welds. Nuclear Waste Management Organization. NWMO TR-2011-03. Toronto, Canada

Wasywich, K.M. and C.R. Frost 1991. Examination of Used CANDU Fuel following 27 years of Storage under Water. 3rd International Conference on Nuclear Fuel Reprocessing and Waste Management (RECOD91). Sendai, Japan.